Progress in Disaster Science 29 (2026) 100512

Contents lists available at ScienceDirect

Progress in Disaster Science

journal homepage: www.elsevier.com/locate/pdisas

# Identifying physical vulnerability drivers increasing in exposed structures to floods

Yelena Hernández-Atencia [a,*], Juanchito Cutupey-Márquez [b], Isabel Rojas [b], Didier Lizcano [b], Jader Muñoz-Ramos [c], Luis E. Peña [b,*]

[a] Research Group AQUA, Faculty of Civil Engineering, Universidad Cooperativa de Colombia, Calle 10 1-120 Edificio Urrutia, 730004 Ibagué, Colombia
[b] GMAE Research Group, Universidad de Ibagué, Carrera 22 calle 67 B/Ambalá, 730001 Ibagué, Colombia
[c] Department of Engineering, Faculty of Forest Engineering, Universidad del Tolima, Barrio Santa Helena Parte Alta, 730006299 Ibagué, Colombia

ARTICLE INFO

*Keywords:*
Flood physical vulnerability
Key factor
Structures exposed to flooding
MICMAC
PCA
CATPCA

ABSTRACT

Diverse structures serve protective functions against floods, yet they remain constantly exposed to water currents, which increase their physical vulnerability. Thus, identifying key factors can be complex given the interrelationships and interactions among hydrological, hydraulic, geomorphological, and many other variables. This study analyzes 13 factors related to the physical vulnerability of structures exposed to flooding from experts' judgment judgment-based approach byCross-Impact Matrix Multiplication Applied to Classification (MICMAC) and multivariate statistics using Principal Components Analysis PCA, and Categorical Principal Component Analysis CATPCA, to highlight the identification of key factors. Subsequently, Spearman's rank correlation coefficient was used to establish metric comparisons between methods. The study evaluated 22 structures along a 20 km stretch of the main channel of the Combeima River in Colombia, using hydrological and hydraulic modeling over a 54-year period (1971–2024), under land-use change scenarios. Results indicate that factors related to the type of cover and the infiltration were highly influential on the level of physical vulnerability. Therefore, the proposed methodology and results can provide elements of judgment for planners in formulating and implementing flood risk management practices.

## 1. Introduction

Floods have the potential to lead to severe consequences for people, infrastructure, and the economy in most mountainous regions worldwide, and the increase in the frequency and intensity of heavy precipitation is expected to worsen local rain-induced flooding [1]. In this sense, over the years 1970 to 2021, 943 disasters attributed to extreme weather events were reported in South America, and of these, 61 % were floods [2]. These disasters resulted in 58,484 deaths and US$115.2 billion in economic losses [3]. In Colombia, between 2000 and 2023, 76 flood disasters were recorded, causing damages estimated at more than US$4.7 billion [4]. Consequently, multiple studies have been carried out to evaluate the capacity of hydraulic structures under non-stationary conditions associated with climate change and land- use change [5], physical flood vulnerability [6], and, more recently, flood vulnerability assessment [7], among many others.

Physical flood vulnerability usually refers to the assessment of flood damage to physical structures [8], that is, the degree of loss of a given element at risk whose characteristics and properties increase its susceptibility to flooding [9]. Additionally, physical vulnerability is directly connected to monetary losses and functional interruptions until the original functionality of affected structures is restored [10]. Thus, it is complex to assess the physical vulnerability of structures given the nonlinear dynamics that emerge between damage and the intensity of the flood event [11].

Various methodologies for estimating the physical vulnerability of structures have been proposed (e.g., [6,12,13]), which incorporate key factors that are weighted within multi-criterion-based analytical hierarchical processes [14], or thematic layers within geographic information systems [15]. However, to the best of the authors' knowledge, few investigations have compared the degree of influence or dependence of these factors on the physical vulnerability processes in structures [16] to determine key factors related to physical vulnerability in structures exposed to flooding. In this sense, approximately 25 % of the surface of the planet is mountainous, where around 12 % of the population lives [17]. Urbanization in the mountains accounts for 66 % of the total, with

* Corresponding authors.
*E-mail addresses:* yelena.hernandez@campusucc.edu.co (Y. Hernández-Atencia), luis.pena@unibague.edu.co (L.E. Peña).

https://doi.org/10.1016/j.pdisas.2025.100512
Received 17 September 2025; Received in revised form 15 December 2025; Accepted 23 December 2025
Available online 31 December 2025

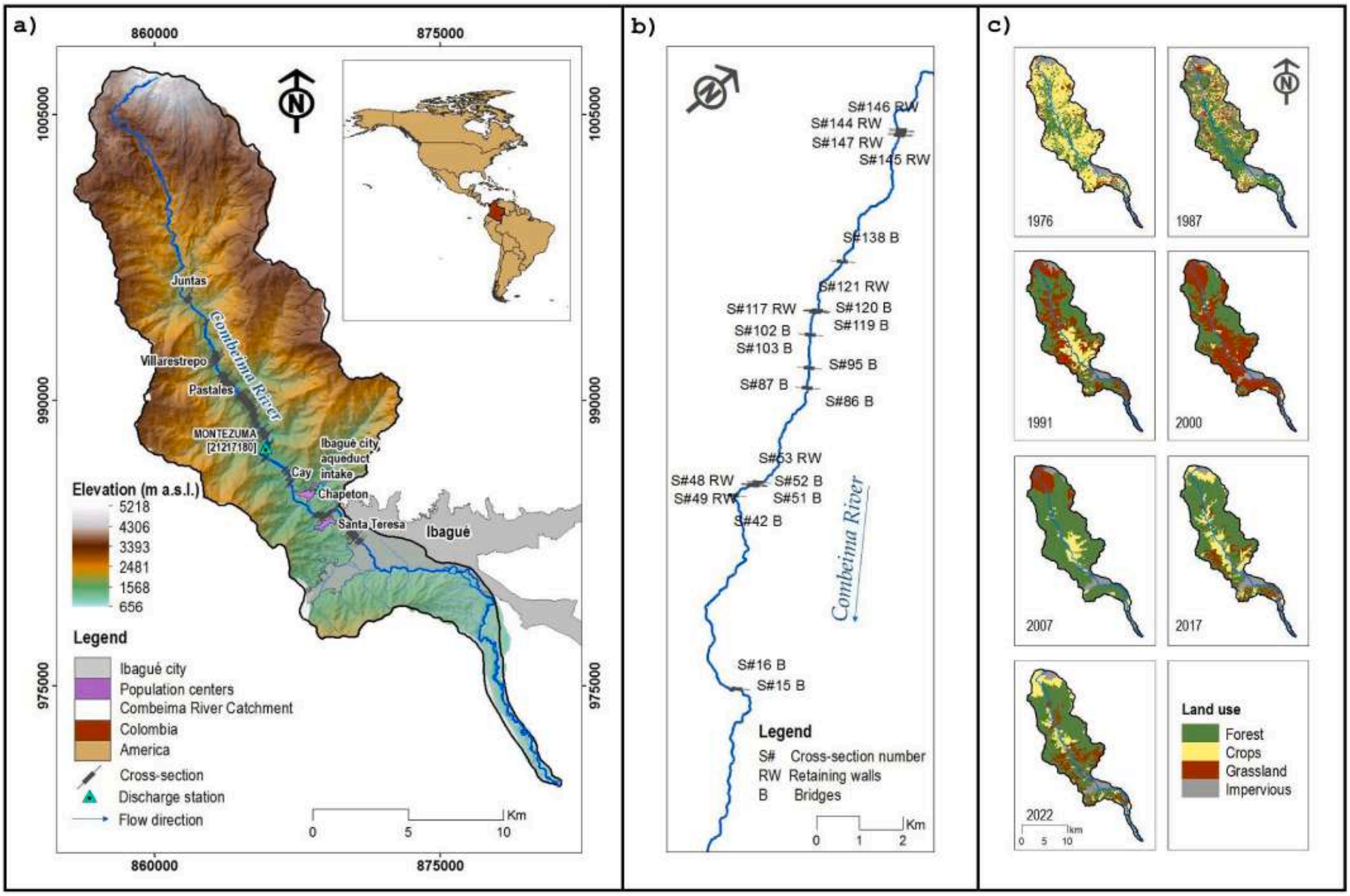


**Fig. 1.** Combeima River catchment: a) Location of the study area; b) Hydraulic modeling cross sections; and c) Land use changes during the 1976–2022 period.

35 % living in cities, while the lowlands are occupied by 78 % of the population [18]. Structures exposed to flooding are very vulnerable, especially in mountain areas, due to the high energy of streams, which are susceptible to land-use and climate changes, depending on their magnitude [19]. Therefore, mountain basins and streams show marked differences compared to lowland basins in factors that determine flooding, such as higher rainfall patterns, slopes, and flow velocities [20,21]. Thus, studies report factors influencing the physical vulnerability of structures exposed to flooding, such as construction materials, previous soil moisture, and soil roughness [9], as well as the natural stability of the streambed [22]. In this sense, there is academic consensus that urbanization is the most determining factor in flood magnitude [23].

In this context, some studies have reported results on the most important factors related to the processes that generate floods. For example, Ariyani et al. [24], using expert judgment and a Cross-Impact Matrix Multiplication Applied to Classification (MICMAC) structural analysis, found that the most influential factors causing flood disasters were land cover/use, slope, population density, and river waste. Similarly, Sharma and Sharma [25] identified rainfall and land use as the flood-generating factors.

On the other hand, the implementation of multivariate techniques using Categorical Principal Components Analysis (CATPCA) has been reported to identify the primary factors associated with the perception of flash flood risk [26]. Likewise, principal components analysis (PCA) has been used to assess the social vulnerability of the Ganga River in India [27] and to deepen understanding of underlying patterns among the main socioeconomic and demographic factors that identify vulnerable populations to urban flooding [28]. Similarly, studies report analyses of factors influencing vulnerability to flooding in mountainous areas of Europe [9,29], Africa [30], where the type of construction material, maximum flow depth, stream width, bed slope, channel slope, maximum flow discharge, flow velocity, concentration time, infiltration, type of vegetation cover, among others, were considered, and very few incorporate multivariate or structural analyses (e.g., [31,32]). Accordingly, the aim of this study is to evaluate the degree of influence of 13 factors related to the physical dimension of flood vulnerability of 22 structures, including bridges and retaining walls exposed to flooding, located along a 20-km stretch of the main stream of the Combeima Catchment, a mountain stream located in the Andes mountain range of Colombia. To this end, the MICMAC, PCA, and CATPCA methods were implemented. In this regard, recent studies have demonstrated the use of MICMAC to identify key factors influencing a hydrological system [33,34]. However, to the best of the authors' knowledge, few studies contrast that type of structural analysis with a statistical analysis. This approach can be useful for developing policies for the protection of life in population centers near streams, which minimize the impact of flooding on the territory [35], especially when damage to bridges and retaining walls is relevant in terms of absolute total costs [36], in addition to the losses caused by interruptions in the development of economic activities that depend on land transportation and the provision of basic services such as drinking water supply.

## 2. Material and methods

### 2.1. Study area

The analysis was conducted in the Combeima River catchment, located in the Colombian Andes, with elevations ranging from 700.6 to 5150.0 m a.s.l., with a mean elevation of 2360.3 m a.s.l., and a surface

**Table 1**
Hydroclimatological events recorded in the Combeima River catchment from 1945 to 2025.

| Date DD/MM/YY | Event type | Event effects | Source |
|---|---|---|---|
| 1945 | Landslides and floods | Some damage to houses, covering part of the village center of Villa Restrepo. | (Espejo-Alfonso, 2021) |
| 29/06/1959 | Landslides and floods | 120 deaths, 350 homeless victims, damage to houses and bridges in Juntas, Villa Restrepo, and the city of Ibagué. | |
| 22/05/1967 | More than 100 landslides and flash floods | One death, loss of crops and livestock. | |
| 21/06/1974 | Landslides and floods | Damage to houses, obstruction, and damage to bridges in the Llanitos and Pastales sectors. | |
| 25/05/1975 | Floods | Damage to the water supply structure of the Cay Sector of the city of Ibagué, loss of crops. | |
| 9/06/1977 | Flash floods | Houses destroyed and flooded, 4 injured in the creek sector of La Plata. | (Consejo Nacional de Política Económica y Social., 2009) |
| 01/06/1980 | Flash floods | 8 houses destroyed in the sector of La Victoria. | |
| 05/11/1981 | Flash floods | 18 houses destroyed in the sector of Chapetón. | |
| 08/06/1984 | Flood | Crop loss at La María farm. | |
| 31/07/1985 | Landslides, Combeima River damming | Houses destroyed and crops lost in the sectors of Juntas and Pastales of the Guamal event. | |
| 04/07/1987 | Landslides and floods | 15 dead, 2300 affected, houses and bridges destroyed, damage to crops, damage to the water supply structure of the city of Ibagué. | |
| 24/06/1989 | Flash flood | 300 dead, damage to houses in the sector of Juntas and the city of Ibagué. | (Espejo-Alfonso, 2021) |
| 14/07/1990 | Landslides, mudflows | Damage to the water supply structure of the city of Ibagué. | |
| 04/06/1991 | Flash flood | 20 houses destroyed, 3 dead, 6 injured. | |
| 05/05/1993 | Combeima River damming | Increase of erosion processes on hillsides. | (Consejo Nacional de Política Económica y Social., 2009) |
| 13/04/1994 | Landslides | One house destroyed, one family affected. | |
| 14/04/1994 | Landslides | 4 dead, one house destroyed. | |
| 20/05/1994 | Torrential rainfalls | Evacuation of families due to house damage. | |
| 1998 | Rock slides | 2 fatalities, destruction of housing, and impacts on the tourist complex. | (Espejo-Alfonso, 2021) |
| 10/09/2000 | Landslides | 14 people affected, 2 families affected. | (Espejo-Alfonso, 2021) |
| 27/05/2002 | Landslides | 10 people affected, 2 families, and 2 houses destroyed. | (Espejo-Alfonso, 2021) |
| 18/11/2004 | Floods | 4 injured, 120 people affected, 24 families, and damaged houses. | (Espejo-Alfonso, 2021) |
| 7/03/2005 | Landslides | 295 people affected, 59 families, and 59 damaged houses. | (Espejo-Alfonso, 2021) |
| 24/06/2006 | Floods | 55 adults and 17 children affected in the sector of Villa Restrepo. | (Olaya-Marín, 2022) |
| 22/08/2008 | Floods | Damage to road infrastructure. | (Espejo-Alfonso, 2021) |
| 01/07/2009 | Flash floods | 170 people affected, damages in more than 40 houses. Damage to the water supply structure of the city of Ibagué for 4 days. Gorges El Salto, Guamal and La seca sectors. | (Ecos del Combeima, 2021) |
| 14/05/2012 | Flash flood | 12 houses damaged in the sectors of Llanitos and Pastales. Damage to the water supply structure of the city of Ibagué. | (Ecos del Combeima, 2012) |
| 04/06/2018 | Flood | Damage to the water supply structure of the city of Ibagué. An event in the sector of Llanitos. | (Alerta Tolima, 2018) |
| 23/11/2021 | Flood | 175 houses damaged, 200 families affected, 5 villages cut off due to road damage. | (Trujillo, 2021) |
| 12/08/2024 | Flood | Damage to the bridge and road in the Villa Restrepo sector, Bellavista stream. | (Redacción Ibagué, 2024) |
| 31/12/2024 | Flood | Damage to the bridge and road in the Puerto Peru sector, Bellavista stream. | (Ecos del Combeima, 2024) |
| 06/04/2025 | Flood | Damage to houses, damage to roads, and mobility in the Villa Restrepo sector. | (Canal PyC, 2025) |
| 28/06/2025 | Flash floods | Damage to the bridge in the Villa Restrepo sector, damage and interruption of the water supply in the city of Ibagué. | (Montiel, 2025) |

area of 273.0 $km^2$, where the average daily and annual precipitations are 4.9 mm and 1768.6 mm, respectively. The catchment has an average gradient of 53.9 %, a drainage density of 1.94 km/$km^2$, and a concentration time of 4.1 h. The main channel is 57.4 km long, with an average gradient of 35.3 %, and a sinuosity of 1.2 km/km. The towns of VillaRestrepo, Pastales, and Llanitos, as well as a water intake structure for the water supply of the city of Ibagué, which has a population of over 546,003 inhabitants, are located along the Combeima River (Fig. 1). Therefore, flooding causes a higher amount of damage and loss of lives, as presented in Table 1. The stream has an average daily flow of 5.7 $m^3$/s, and the maximum annual flow is 77.5 $m^3$/s, according to the Montezuma Hydrometric Station records for the 1971 to 2024 period (Fig. 1a). For the hydraulic analysis, 150 cross sections were used in a 20.0 km stretch between VillaRestrepo and Ibagué (Fig. 1b), where 22 structures are exposed to flooding, of which 13 correspond to bridges and 9 to retaining walls. Finally, vegetation cover maps that record land use changes (LUC) during the years 1976, 1987, 1991, 2000, 2007, 2017, and 2022 were employed (Fig. 1c). Therefore, the definition of the river reach analyzed considered the existence of structures for the protection of human settlements located in the riparian zone, road infrastructure, drinking water supply structures, and agricultural areas that are related to the criteria and goals established in the Framework for Disaster Risk Reduction 2015–2030 [37].

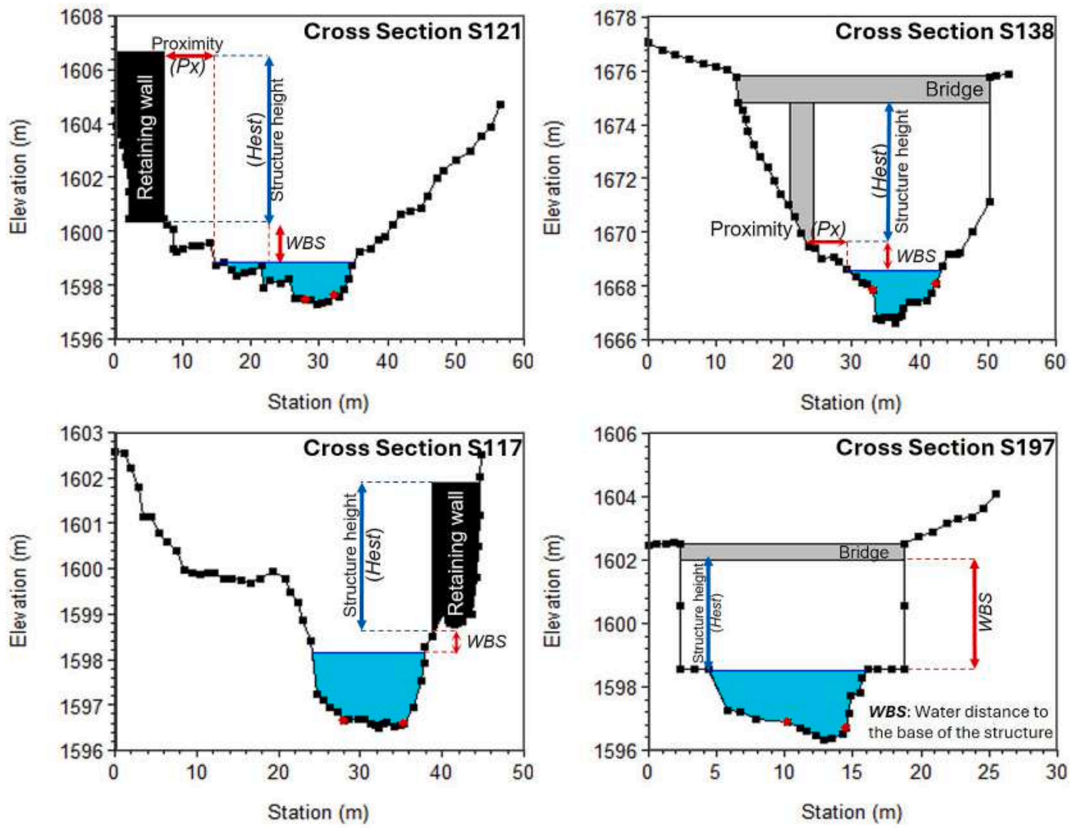


**Fig. 2.** Descriptive example of the measurement of proximity (Px) and structure height (Hest) in retaining walls and bridges. WBS is the water distance to the base of the structure.

### 2.2. Influencing factors

This study reviewed factors generating flooding in watersheds, which are dependent on climate and hydrology [38], such as rainfall characteristics, watershed morphology [39], land-use changes, and climate change [40,41], among others. Likewise, factors influencing the physical vulnerability of structures were defined as those that can increase damage to a structure [42] or its susceptibility [43,44], such as: type of structure, location, exposure, as well as construction materials and condition of the structure [45], as well as the horizontal and vertical distance to the stream [46,47]. On this basis, a review of the academic literature was conducted,and 13 factors were selected through expert judgment [48] to assess their level of influence on the physical vulnerability of structures exposed to flooding. These factors were chosen based on their relationship with the physical vulnerability of structures and flood propagation. The experts included professors from Universidad Cooperativa de Colombia, Universidad de Ibagué, Universidad del Tolima, and government officials specialized in flood risk management in the study area. These factors are classified into three groups, based on their relationship with catchment variables, structures, and the current. In this sense, recent studies recognize the capacity of expert judgment in the selection processes of variables that influence the response of hydrological systems (e.g., [33,34,49,50]). Therefore, the experts' criteria were complemented by a review of relevant academic literature, which provides justification for selecting 13 influential factors affecting the physical vulnerability of structures exposed to flooding (Section 2.2). These factors allow identifying the effects of floods on the vulnerability and potential damage to vital infrastructure, such as roads and water supply systems of population centers in the area analyzed in this study, which is consistent with the goals defined in the Sendai Framework for Disaster Risk Reduction 2015–2030 [37]. Thus, in this study, the 13 factors selected were classified into three categories: i) catchment; ii) stream; and iii) structure-related factors, similar to the source-pathway-receptor framework widely used in flood vulnerability [33]. Furthermore, the proposed methodology requires knowledge of the variable values for each structure in each simulated land-use change scenario; therefore, some variables were adapted or discarded based on their availability. Finally, there is no widely accepted paradigm for identifying the most appropriate factors; therefore, a small set of well-chosen factors provides results without unnecessary complications [50].

#### 2.2.1. Catchment-related factors

Multiple studies describe the importance of precipitation (P) in producing surface runoff, and particularly extreme rainfall converges with multiple drivers that exacerbate flooding [51]. Thus, increases in peak flow magnitude are driven primarily by changes in extreme precipitation [52]. Likewise, discharge (*Q*) is the reference variable in flood analysis with exposed structures, and is related to peak flow and the return period [53]. Besides, it is highly dependent on rainfall [54]. The curve number (*CN*) was also considered because of its high relationship with LUC and land cover in surface runoff production processes, and has been used for flood susceptibility mapping [55], due to its relationship with extreme rainfall [56]. Therefore, the CN has been considered as one of the main drivers of flood generation in LUC scenarios [57]. In this study, LUC and land cover factors were represented through the curve number proposed by the Natural Resources Conservation Service (NRCS), previously known as the SCS-CN [58]. Similarly, other studies have used the *CN* to obtain flood depths [59].

To relate the edaphology of the catchment within the runoff generation process, the soil water storage in the root zone ($H_u$), also known as static storage, was considered, and is represented in this study according to the conceptualization of Francés et al. [60] as follows (Eq. 1).

$$H_u = \sum_i h_i AW_i + I_{max} + A_s \quad (1)$$

where the difference between the field capacity and wilting point corresponds to the depth $h_i$(mm) of the available water $AW_i$(mm) in each soil horizon, so the sum is carried out until the minimum value between the soil depth and the effective root depth is reached. Then, $I_{max}$ represents the maximum interception of the canopy (mm), and $A_s$ is the maximum surface depression storage (mm). Studies have reported that $H_u$ varies due to changes in soil permeability, affecting the production of surface runoff [61,62], which influences the level of vulnerability of structures exposed to flooding, especially when soil permeability is low [56]. Likewise, static storage in watersheds has been reported as perhaps the most influential variable in flood analysis in changing land use environments [63].

On the other hand, during the occurrence of floods, water depth, flow velocity, and shear stress in the current increase, generating sediment removal and transport in the channel [64], and can cause destabilization of structures exposed to flooding due to scour around them [65]. Thus, variations in the cross-section shape contribute to the increased susceptibility of structures exposed to flooding [53]. In this study, to represent these effects, the potential erosion factor (Pe) was defined, which corresponds to the unitary flow of sediments $q_t$ (t/m*s) generated in the catchment with a closure point in the cross section where the structure $S_i$ is located in a stream of water $Q$ per unit of width $W$, and according to Julien [66], it is represented as Eq. 2.

$$q_t = 25500\, S_0^{4366} \left(\frac{Q}{W}\right)^{2.035} \frac{K}{0.15} C\, P \quad (2)$$

where $K, C,$ and $P$ correspond respectively to the soil erosibility, cultivation, and conservation practices, factors of the Universal Soil Loss Equation USLE [67].

### 2.2.2. Structure-related factors

Structure proximity to the water stream (*Px*) corresponds to the distance from the stream to the exposed structure (Fig. 2), which is a counting factor in flood risk models [68] and is influential on the effects on exposed structures (e.g., [24,68]). Likewise, material type (*MT*) was considered because it is one of the factors that control the failure of structures during large floods [65,69]. Structure height (*Hest*) is related in the vulnerability analysis to the level of hazard (e.g., floodwater depth) on the structures exposed to flood conditions (Fig. 2). In this sense, the height of the exposed structure can determine its potential disruption in a flood event [70].

### 2.2.3. Stream-related factors

The flood area (*A*) has been used in various studies as a measure of flood vulnerability assessment [71], and in some studies, it is incorporated as a factor of flooded area in the vulnerability analysis of structures [56]. Likewise, shear stress (*T*) was considered since currents subject exposed structures to significant shear forces that can lead to their failure [68] and, therefore, influence their stability [64]. In this sense, flood depth (*H*) has been included because floodwater height determines the severity of the impact on structures exposed to flooding [65], so physical vulnerability is highly related to flood depth [36]. For bridges in flood zones, they are considered vulnerable when the flood depth is equal to or exceeds the lower deck height [52]. Flow velocity (*V*) was included because structures exposed to flooding can suffer significant damage when faced with high velocity flows [65], especially to the scour around its foundation [53], which can also alter the geometry of the cross section and the riverbed (*S*), which influences the spread of floods [72]. In some cases, even with normal rainfall, the riverbed may tend to rise its level, causing widespread flooding [73]. In other cases, sediment is extracted to restrict flood depth and thus minimize flooding potential [74]. Therefore, morphological variations in the riverbed near an exposed structure can significantly alter its stability and physical vulnerability [75].

**Table 2**
Methodologies implemented for the assessment of the physical vulnerability of structures to flooding in LUC scenarios.

| Methodology | Description and approach | Equation | Variables | | Variables description |
|---|---|---|---|---|---|
| VFVCN | Assessment of physical vulnerability based on changes in runoff, infiltration, and flow velocity in the channel. | $V_{ij} = E_{ij}{*}S_{ij}$ | $I_{ij} = v$ | $S_{ij} = CN$ | Here, variable *I* is the intensity of the event, *S* corresponds to susceptibility, while v indicates the maximum flow velocity in the cross section, and *Hu* represents water storage in the soil in the root zone. |
| VVHu | Assessment of physical vulnerability based on changes in soil water storage in the root zone due to changes in land use and flow velocity in the channel. | $V_{ij} = I_{ij}{*}S_{ij}$ | $I_{ij} = v$ | $S_{ij} = \frac{1}{Hu}$ | |
| MFLUP | Assessment of physical vulnerability based on the measurement and mapping of land use patterns. | $V_{ij} = E_{ij}{*}S_{ij}$ | $E_{ij} = \frac{1}{Px_{ij}}$ | $S_i = \frac{h_{ij}}{H_{est_{ij}}}$ | *E* represents exposure, *Px* is the distance from the stream to the exposed structure, *S* is susceptibility, *h* is water depth, and the height of the exposed structure is $H_{est}$. |
| VLUCS | Assessment of physical vulnerability in land use change scenarios based on Morpho-Edaphological Attributes of the basin. | $V_{ij} = a(St_{ij}) + b(A_{ij}) + c(Sc_{ij}) + d(LUC)$ | | | *St* is soil type of basin area, *A*, represents basin area, *Sc* is the slope of the basin within the area corresponding to the exposed structure, *LUC* is land use change, and coefficients $a, b, c$, y $d$ are the weights of each variable. |

## 2.3. Hydrological and hydraulic modeling

To describe runoff behavior, a physically based tank conceptualization was implemented, incorporating the spatially distributed hydrological model TETIS [60], which also allows modeling sediment yield [76], in changing land use scenarios [62]. Thus, LUC were modeled from the land use maps in the Combeima River catchment corresponding to the years 1976, 1987, 1991, 2000, 2007, 2017, and 2022 (Fig. 1a-c), and hydroclimatological information from the catchment recorded during the 1971–2024 period with daily temporal resolution, which allowed obtaining the maximum flows and sediment concentrations in each scenario. To evaluate the descriptive capacity of the model, acceptable calibration was defined as Nash-Sutcliffe objective function values higher than 5.0 [77].

The hydraulics of the Combeima River over a 20 km stretch between the towns of Villa Restrepo and Ibagué were represented through the implementation of HEC-RASv6.6 [78]. The system schematization consists of 150 cross sections containing 13 bridges and 9 retaining walls (Fig. 1a-b). The boundary conditions correspond to the maximum flows for a 100-year return period during the years with recorded land-use changes, i.e., 1976, 1987, 1991, 2000, 2007, 2017, and 2022. The frequency analysis was performed with the General Extreme Values function, which has been widely used in the study area (e.g., [63]). The model was considered calibrated for percent bias (PBIAS) in water depth values below 20.0 % by adjusting the roughness coefficient in each cross section [79]. Thus, negative values indicate that the simulated value is higher than the observed value; positive values indicate that the simulated water depth is lower than the observed value [80].

### 2.4. Physical vulnerability methods and data

In general vulnerability has been defined as propensity or predisposition to be adversely affected, which includes the concept of sensitivity or susceptibility to damage [81]. In this sense, the Sendai Framework states the need to improve understanding of disaster risk from dimensions such as exposure, vulnerability, and hazard characteristics [37]. Herefore, in this study, physical vulnerability is considered as a function of exposure ($E$) and susceptibility ($S$), where a structure has a pre-existing condition of exposure to flooding, which, according to its physical characteristics, interacts with the dynamics of a stream in a changing land use environment, which could increase its susceptibility. Likewise, this study focused on analyzing the physical vulnerability of structures exposed to flooding, such as retaining walls and bridges located on the Combeima River, without considering social, cultural, economic, legal, or institutional dimensions, similar to the approach proposed by Papathoma-Köhle et al. [9] for the assessment of alpine hazards. Therefore, based on the hydrological and hydraulic modeling results, four methods were implemented to estimate physical vulnerability to flooding: i) Vulnerability Based on Flow Velocity and Curve Number (VFVCN); ii) Vulnerability Based on Soil Water Storage Variation (VVHu), both proposed by Hernández-Atencia et al. [6]; iii) Vulnerability and Mapping of Floods Based on Land-Use Patterns (MFLUP) [13]; and Vulnerability in Land-Use Change Scenarios (VLUCS) based on morpho-edaphological attributes constructed by Caldas et al. [12].

Therefore, Table 2 presents a description of the implemented methodologies, where the term $V_{ij}$ corresponds to the physical vulnerability of structure $i$, located in cross-section $j$ of the channel, exposed to flooding. Furthermore, in this study, the physical vulnerability levels of structures in each method were determined based on water depth using the total height of the exposed structure. Thus, a low level of physical vulnerability indicates a water depth of less than 33 % of the height of the exposed structure, while medium vulnerability occurs when water depth ranges from 33 to 66 % of the height of the structure, and a water depth greater than 66 % determines a high level of vulnerability.

### 2.5. Cross-impact matrix multiplication applied to classification (MICMAC)

To analyze the influence and dependence of the factors selected in this study on the physical vulnerability of structures exposed to flooding, the MICMAC (for its French acronym) structural analysis [82] was implemented. The method allowed identifying key factors that drive the system [83], based on the matrix multiplication properties; the analysis results classify the factors into four categories: autonomous, linkage, dependent, and independent factors [84]. In this study, six experts participated in the process without communicating with one another, thereby reducing bias during the evaluation. The group included university professors and government officials involved in disaster risk management, familiar with flood analysis in mountain basins. The MICMAC software was used to process the ratings [85], facilitating the response analysis. Therefore, expert judgment defined the degree of influence that a factor has on other factors; that is, 169 pairs of pairwise factors were described in a structural analysis matrix called the direct influence matrix. In this sense, a value of 0 means no influence between factors; values of 1 and 2 represent weak and moderate influence, respectively; and a value of 3 means a strong influence [49]. Therefore, a MICMAC structural analysis was conducted to identify the most important factors related to physical vulnerability in structures exposed to flooding, similar to that carried out by Ariyani et al. [24] and Sharma and Sharma [25].

Ratings made using expert judgment involve a subjective comparison process. Therefore, the uncertainty of the Direct Influence Matrix (DIM) (Table 4) was evaluated, where non-diagonal elements were treated as random variables bounded by their minimum, maximum, and most probable values. Each DIM rating was approximated by using the beta-PERT distribution via pseudo-random number generation in Python, yielding 100,000 samples to model expert judgment through Monte Carlo simulations [86]. This approach has been used in risk analysis studies due to its accuracy in estimating the most probable values (e.g., [87]).

### 2.6. Principal components analysis (PCA)

A principal components analysis (PCA) allows to reduce the dimensionality between intercorrelated numerical variables [55], and applies an orthogonal transformation to convert a data set into uncorrelated variables called principal components [88], where the eigenvalues are the explained variance, and the highest weighted components of the data set can be identified [73]. In that sense, a PCA approach with 12 of the factors described in section 2.2. (excluding the categorical variable material type because it cannot be transformed into an equivalent numeric value by this method) and each method for estimating physical vulnerability in structures was performed to identify the most significant variable in the processes of physical vulnerability in structures exposed to floods, similar to the approach taken by Langlois et al. [71] and Narendra et al. [55]. However, it should be noted that the method has limitations, as it assumes linear relationships between variables [65], whereas hydrological processes exhibit nonlinear behavior [89].

### 2.7. Categorical principal components analysis (CATPCA)

Categorical variables that define levels of physical vulnerability were included in the analysis, so it was necessary to use categorical principal components analysis (CATPCA), which reduces the dimensionality of intercorrelated categorical and numerical variables. This method is the nonlinear equivalent of a conventional PCA and reduces observed variables to uncorrelated principal components [90]. That is, it does not assume linear relationships between categorical and numerical data in a normalized data set [26]. In that sense, a CATPCA approach with the 13 factors described in section 2.2, and each of the methods to estimate the physical vulnerability in structures, was carried out to identify the most significant variable in the processes of physical vulnerability in structures exposed to floods, similar to that reported by Martins and Nunes [26]. The PCA and CATPCA were performed in the program IBM SPSS Statistics for Windows, Version 25.0.

### 2.8. Validation of influential factors

To contrast the results of the influence analysis obtained using MICMAC, PCA, and CATPCA, influential factors were defined as those with the four highest positive driver values and the lowest dependence in the case of MICMAC [84]. Results from PCA and CATPCA were analyzed using a vulnerability correlation matrix, and the factors with the four highest positive and negative correlations were selected as influential. That is, correlations (r) with values $r > 0$ are directly proportional; $r < 0$ is inversely proportional; $r \cong 0$ indicates that the variable is independent [91]. Therefore, in this study, PCA results with

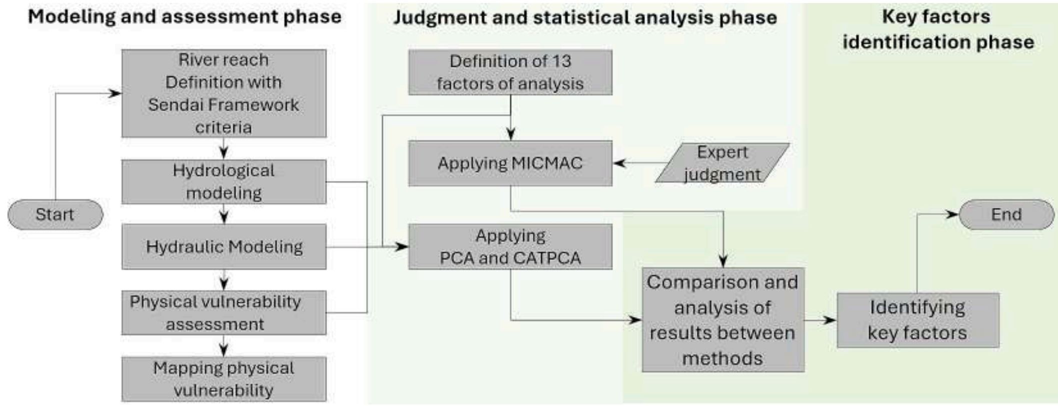


**Fig. 3.** Process applied to identify key factors in the evaluation of the physical vulnerability of structures exposed to flooding.

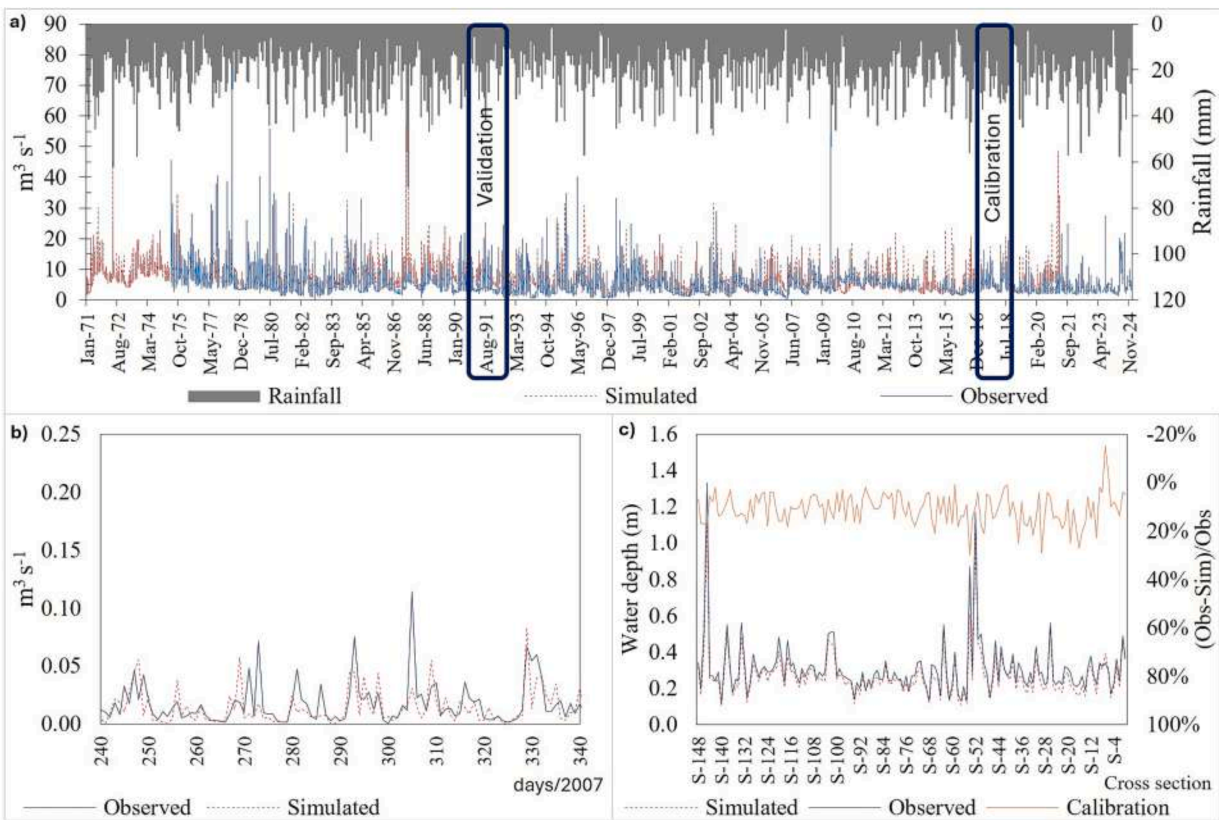


**Fig. 4.** a) Hydrological model calibration/validation; b) Sediment submodel calibration; and c) Hydraulic model calibration.

correlations of $r > 0.50$ and $r < -0.50$ are considered as driving variables or key factors, and for CATPCA, correlations of $r > 0.255$ and $r < -0.25$. Furthermore, given this analysis of the findings is presented in a hybrid framework integrating structural analysis (MICMAC) with data dimensionality reduction techniques such as PCA and CATPCA, a quantitative assessment of convergence or divergence is required, highlighting a gap in the literature due to the lack of a standardized protocol for statistically comparing the results of expert-based and data-based models. Therefore, we performed a comprehensive derivation of Spearman's Rank Correlation Coefficient (ρ) [92] to establish comparisons using metrics among the three methods used in this study. To this end, the convergence levels ($R$) reported by Caruso and Clieff [93] were used, where: Very strong $R_{vs} = \{\rho \in \mathbb{R} | 0.80 \le |\rho| \le 1.0\}$, Strong $R_s = \{\rho \in \mathbb{R} | 0.60 \le |\rho| \le 0.79\}$, Moderate $R_m = \{\rho \in \mathbb{R} | 0.40 \le |\rho| \le 0.59\}$, Weak $R_w = \{\rho \in \mathbb{R} | 0.20 \le |\rho| \le 0.39\}$, Very weak $R_{vw} = \{\rho \in \mathbb{R} | 0.00 \le |\rho| \le 0.19\}$, where $p$-values $<0.05$ were considered statistically significant. This scale has been successfully applied in flood studies (e.g., [94]).

Finally, Fig. 3 summarizes the methodological process applied in this study.

## 3. Results

### *3.1. Hydrologic and hydraulic modeling of the system*

During the hydrological model calibration process, the Nash-Sutcliffe index values were 0.61 for calibration and 0.56 for validation, corresponding to the years 2017 and 1991, respectively. The hydraulic model also obtained a PBIAS of 11.0 % (Fig. 4). Therefore, since the implemented models are mostly physically based and adequately

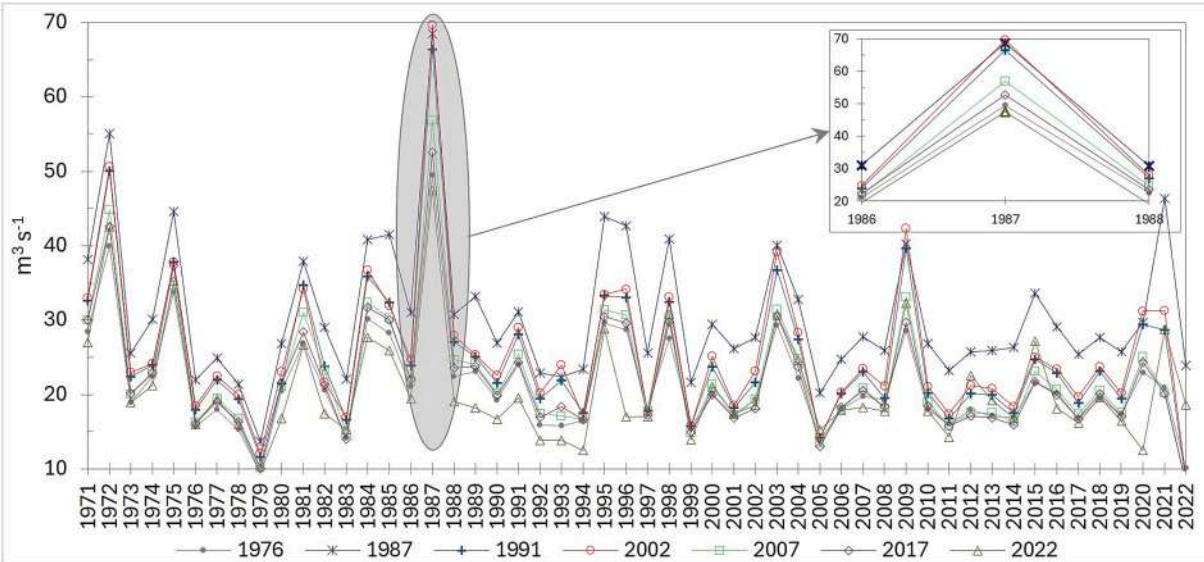


**Fig. 5.** Annual maxima in LUC scenarios.

**Table 3**
Land use/cover changes during the 1976–2022 period.

| Land use /cover | Land-use change per year ($km^2$) | | | | | | |
|---|---|---|---|---|---|---|---|
| | 1976 | 1987 | 1991 | 2000 | 2007 | 2017 | 2022 |
| Forest | 73.7 | 136.4 | 138.4 | 100.9 | 201.4 | 172.4 | 170.4 |
| Crops | 162.5 | 60.3 | 32.5 | 8.7 | 27.7 | 55.4 | 45.4 |
| Grassland | 18.6 | 32.8 | 90.6 | 150.6 | 27.4 | 24.3 | 37.1 |
| Impervious | 18.2 | 43.4 | 11.4 | 12.8 | 16.5 | 20.9 | 20.1 |
| $H_u$ (mm) | 63.7 | 88.0 | 86.5 | 86.5 | 86.5 | 86.5 | 66.3 |
| *CN* | 58.2 | 57.9 | 57.4 | 58.3 | 49.3 | 40.4 | 37.6 |
| Qmax ($m^3/s$) | 49.5 | 68.5 | 66.4 | 69.6 | 56.8 | 52.6 | 47.4 |

describe water behavior in the catchment, their results were useful for analyzing the influence and interaction of the 13 factors selected in this study in the assessment of the physical vulnerability of structures exposed to flooding.

From the hydrological modeling, the annual maximums corresponding to the land-use change maps of the years 1976, 1987, 1991, 2000, 2007, 2017, and 2022 were obtained. During the 1987–1991-2000 period, areas with grassland cover increased, also increasing maximum flows. Notably, 1976 had the smallest forest area and the lowest soil water storage during the entire modeled period. In contrast, during the 2007–2017-2022 period, an increase in forest areas was recorded, along with decreases in grassland areas and in the ***CN*** from 49.3 to 37.6, which led to reduced runoff and maximum flows in the river (Figs. 1 and 5, Table 3). This confirms that the trend towards basin impermeability from deforestation or urbanization contributes to increased peak flows by reducing infiltration [95]. Thus, the transition from grassland to forest contributes to the attenuation of peak flows and reduces the risk of flooding [96].

### 3.2. Change in physical vulnerability due to LUC during 1976–2022

Since alterations in infiltration in watersheds influence runoff generation in LUC scenarios [95], the resulting water depth in a cross-section interacts with stream structures, determining their level of vulnerability. Therefore, the physical vulnerability of structures exposed to flooding was evaluated using four conceptualizations (Table 2). Changes in the level of vulnerability were found in structures such as bridges and retaining walls, as presented in Fig. 6, where MFLUP presents high levels of physical vulnerability in the lower part of the analyzed river reach (sections S#52B–S#15B) during 2017, represented in red, even though during the 2007–2022 period the largest forest area, the highest soil water storage capacity ($H_u$), and the lowest runoff generation were recorded, corresponding to low *CN* values (Table 3 and Fig. 5). Subsequently, VLUCS defines high vulnerability in 2017 for structures located between S#52B and S#15B (Fig. 6), when the largest forest area is found. The lowest peak flows were obtained through hydrological modeling (Figs. 5 and 6), indicating a poor representation of vulnerability based on land-use changes. However, VLUCS successfully represents the transition from high to medium physical vulnerability, depicted in yellow for the same river reach in 2007 and 2022, consistent with the increase in forest and crop cover (Table 3).

On the other hand, the physical vulnerability levels of structures obtained with VFVCN provide a better approximation of changes in the *CN* during the modeled years. However, between S#120B–S#119B and S#52B–S#42B, low vulnerability levels (in green) are present in the 2000 scenario, where the highest peak flow in the modeled series occurs (69.6 $m^3/s$). High physical vulnerability is observed in the 2017–2022 period across the same river reaches, despite the lowest peak flows of 52.6 and 47.4 $m^3/s$, respectively (Fig. 5 and Table 3).

Finally, VVHu represents physical vulnerability consistently in land-use change scenarios compared to the other methods. In this sense, between S#42B and S#15B, a transition from medium physical vulnerability in 2017 to high in 2022 is observed (Fig. 6), when crop areas decrease by 20 % and grassland areas increase by 35 % in the middle and lower part of the basin (Fig. 1 and Table 3), influencing the increase in flow velocity in the channel, which incorporates the equation that describes the method (Table 2).

### 3.3. MICMAC analysis of direct and indirect interactions

From the direct influence matrix generated through expert judgment [48] (Table 4), the influence of the first factor (1Q list of rows) is observed over the second factor (2Px list of columns) with a value of zero (0), which indicates the absence of influence. Therefore, values of 1 and 2 indicate weak and moderate influence, respectively, while 3 indicates strong influence. Likewise, the indirect influence matrix (Table 5) corresponds to the fifth power of the influence matrix, where the hierarchy of dependence and influence was stabilized, as proposed by Godet [84].

According to Godet [84], the factors were classified based on their influence and dependence. Thus, the analyzed factors were placed in four quadrants: i) in the upper left quadrant are the independent factors


**Fig. 6.** Evolution of physical vulnerability in scenarios of LUC in the analyzed river reach.

**Table 4**
Direct Influence Matrix (MDI).

| Factor | 1*Q* | 2*Px* | 3*CN* | 4$H_u$ | 5*Pe* | 6*A* | 7*H* | 8*V* | 9*T* | 10*S* | 11*MT* | 12*Hest* | 13*P* | Driver Power |
|---|---|---|---|---|---|---|---|---|---|---|---|---|---|---|
| 1*Q* | 0 | 2 | 0 | 0 | 3 | 3 | 2 | 3 | 2 | 1 | 2 | 3 | 0 | 21 |
| 2*Px* | 0 | 0 | 0 | 0 | 2 | 2 | 2 | 2 | 2 | 1 | 3 | 3 | 0 | 17 |
| 3*CN* | 3 | 1 | 0 | 0 | 2 | 2 | 3 | 2 | 2 | 1 | 2 | 2 | 0 | 20 |
| 4$H_u$ | 3 | 1 | 2 | 0 | 1 | 3 | 3 | 3 | 2 | 0 | 1 | 2 | 0 | 21 |
| 5*Pe* | 0 | 1 | 0 | 0 | 0 | 1 | 1 | 1 | 2 | 2 | 3 | 1 | 0 | 12 |
| 6*A* | 0 | 3 | 1 | 0 | 2 | 0 | 3 | 2 | 2 | 1 | 2 | 3 | 0 | 19 |
| 7*H* | 0 | 3 | 1 | 0 | 3 | 3 | 0 | 3 | 3 | 1 | 3 | 3 | 0 | 23 |
| 8*V* | 0 | 3 | 0 | 0 | 3 | 3 | 2 | 0 | 3 | 2 | 3 | 2 | 0 | 21 |
| 9*T* | 0 | 3 | 0 | 0 | 3 | 2 | 0 | 0 | 0 | 1 | 3 | 1 | 0 | 13 |
| 10*S* | 0 | 1 | 0 | 0 | 2 | 2 | 3 | 3 | 2 | 0 | 2 | 2 | 2 | 19 |
| 11*MT* | 0 | 3 | 0 | 0 | 0 | 0 | 0 | 0 | 0 | 0 | 0 | 3 | 0 | 6 |
| 12*Hest* | 0 | 0 | 0 | 0 | 0 | 3 | 0 | 0 | 0 | 0 | 3 | 0 | 0 | 6 |
| 13*P* | 3 | 1 | 0 | 0 | 2 | 1 | 2 | 1 | 1 | 1 | 2 | 1 | 0 | 15 |
| Dependence Power | 9 | 22 | 4 | 0 | 23 | 25 | 21 | 20 | 21 | 11 | 29 | 26 | 2 | |

*Q*: Discharge, *Px*: Structure proximity to water stream, *CN*: Curve number, $H_u$: Soil water storage in the root zone, *Pe*: Potential erotion, *A*: Flood area, *H*: Flood depth, *V*: Flow velocity, *T*: Shear stress, *S*: Riverbed, *MT*: Material type, *Hest*: Structure Height, and *P*: Precipitation.

with high influence and low dependence or driving factors; ii) in the upper right quadrant are the linkage factors with high influence and high dependence or linkage factors; iii) in the lower right quadrant are the variables called dependent factors with low influence and high dependence; and iv) in the lower left quadrant are the independent factors with low influence and low dependence. Likewise, the variables that are moderately motor, dependent, or both, are located in the gray zone, for which there is no analyzable result. In this sense, the results obtained with MICMAC indicated that the key factors or driving factors in the physical vulnerability of structures exposed to floods were: soil

**Table 5**
Indirect influence matrix (MII).

| Factor | 1Q | 2Px | 3CN | $4H_u$ | 5Pe | 6A | 7H | 8V | 9T | 10S | 11MT | 12Hest | 13P | Driver Power |
|---|---|---|---|---|---|---|---|---|---|---|---|---|---|---|
| 1Q | 4044 | 108,717 | 11,919 | 0 | 86,124 | 97,754 | 67,027 | 64,106 | 80,321 | 48,797 | 138,140 | 120,470 | 7058 | 834,477 |
| 2Px | 3012 | 80,000 | 8768 | 0 | 63,408 | 71,909 | 49,545 | 47,199 | 59,172 | 35,990 | 101,807 | 88,797 | 5172 | 614,779 |
| 3CN | 4371 | 113,527 | 12,406 | 0 | 90,264 | 102,697 | 70,266 | 67,076 | 84,247 | 51,240 | 145,028 | 126,042 | 7344 | 874,508 |
| $4H_u$ | 5019 | 131,172 | 14,347 | 0 | 104,269 | 118,502 | 81,121 | 77,621 | 97,293 | 59,136 | 167,408 | 145,652 | 8544 | 1,010,084 |
| 5Pe | 2268 | 57,978 | 6350 | 0 | 46,296 | 52,798 | 36,084 | 34,464 | 43,272 | 26,308 | 74,568 | 64,640 | 3744 | 448,770 |
| 6A | 3663 | 98,233 | 10,760 | 0 | 77,594 | 87,961 | 60,415 | 57,574 | 72,336 | 44,020 | 124,400 | 108,512 | 6326 | 751,794 |
| 7H | 4140 | 112,324 | 12,339 | 0 | 88,982 | 100,963 | 69,257 | 66,435 | 83,006 | 50,373 | 142,715 | 124,625 | 7328 | 862,487 |
| 8V | 3939 | 103,120 | 11,288 | 0 | 81,996 | 93,409 | 63,714 | 60,968 | 76,557 | 46,505 | 131,769 | 114,501 | 6676 | 794,442 |
| 9T | 2184 | 57,962 | 6336 | 0 | 46,296 | 53,000 | 35,686 | 34,488 | 43,152 | 26,102 | 74,352 | 64,486 | 3816 | 447,860 |
| 10S | 3870 | 102,639 | 11,243 | 0 | 81,386 | 92,277 | 63,476 | 60,633 | 75,915 | 46,152 | 130,582 | 113,904 | 6678 | 788,755 |
| 11MT | 783 | 23,559 | 2607 | 0 | 18,180 | 20,454 | 14,094 | 13,413 | 16,920 | 10,305 | 28,977 | 25,539 | 1476 | 176,307 |
| 12Hest | 1071 | 25,236 | 2748 | 0 | 20,736 | 24,066 | 16,035 | 15,615 | 19,419 | 11,703 | 33,648 | 28,812 | 1698 | 200,787 |
| 13P | 3288 | 84,790 | 9251 | 0 | 67,557 | 77,014 | 52,478 | 50,180 | 63,040 | 38,318 | 108,575 | 94,207 | 5500 | 654,198 |
| Dependence Power | 41,652 | 1,099,257 | 120,362 | 0 | 873,088 | 992,804 | 679,198 | 649,772 | 814,650 | 494,949 | 1,401,969 | 1,220,187 | 71,360 | |

*Q*: Discharge, *Px*: Structure proximity to water stream, *CN*: Curve number, $H_u$: Soil water storage in the root zone, *Pe*: Potential erotion, *A*: Flood area, *H*: Flood depth, *V*: Flow velocity, *T*: Shear stress, *S*: Riverbed, *MT*: Material type, *Hest*: Structure Height, and *P*: Precipitation.

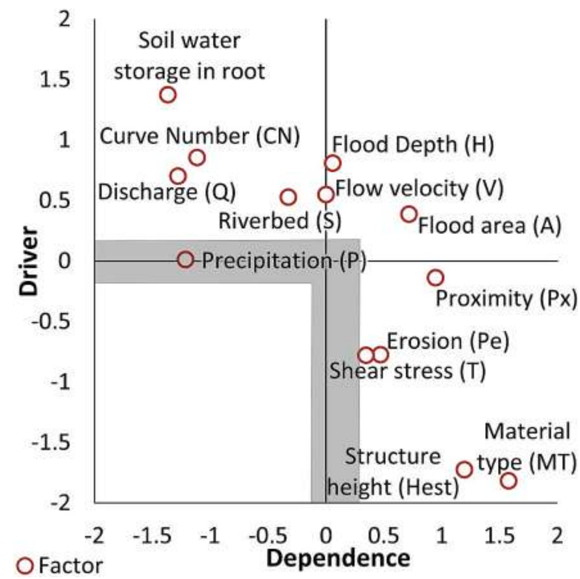


**Fig. 7.** Influence-dependence relationship of physical vulnerability factors in structures exposed to flooding conditions.

water storage in the root zone (***$H_u$***), curve number (***CN***), discharge (***Q***), and riverbed (***S***). The following linkage factors were then obtained: flow velocity (***V***), flood depth (***H***), and flood area (***A***). Finally, the dependent factors were material type (***MT***), structure height (***Hest***), potential erosion (***Pe***), and shear stress (***T***) (Fig. 7).

From a Bayesian perspective, expert judgment introduces subjectivity because their ratings correspond to prior distributions. Therefore, a calibration was performed in which 100,000 DIMs were generated using a Monte Carlo simulation. This revealed an overestimation in the experts' ratings (Fig. 8) that was not apparent in the initial analysis (Fig. 7), thus highlighting the importance of considering this subprocess. In this regard, the consistency of the pairwise evaluation was determined using the consistency ratio (*CR*). This is $CR = CI/RI$; where the random index *RI* depends on the size of the pairwise comparison matrix and was 1.8749, and a value of 0.0729 was obtained for the consistency index calculated as $CI = (\lambda_m - n)/(n-1)$, where $\lambda_m$ is the eigenvalue obtained from the sum of products between each element of the vector of eigenvalues and the sum of the column of the direct influence matrix, which has a size of $n = 13$ (Tables 4 and 5). Thus, the results are considered valid when $CR \leq 0.1$ [97]. In this study, $CR = 0.0467$ was obtained, and therefore MICMAC results are highly consistent with the Driver and Dependence value vectors obtained through the Monte Carlo simulation, and the variations were marginal (Fig. 8).

### 3.4. Correlation analysis with PCA

In this study, four physical vulnerability methods were implemented to analyze 22 structures exposed to flooding: VFVCN, VVHu, MFLUP, and VLUCS. Dimensionality reduction was performed by selecting the first two principal components (PC1 and PC2) using PCA [50]. In Fig. 9a, the first component is highly correlated with curve number (*CN*), VFVCN, and discharge (*Q*), and the second component is strongly correlated with flood extension (*A*), flow velocity (*V*), and flood depth (*H*). For Fig. 9b, PC1 is strongly correlated with VVHU, discharge (*Q*), and curve number (*CN*), and PC2 is highly correlated with flood extension (*A*) and flood depth (*H*). Similarly, in Fig. 9c, PC1 is mainly correlated with flood velocity (*V*) and flood extension (*A*), and PC2 is mainly correlated with curve number (*CN*) and discharge (*Q*). Finally, Fig. 9d shows that PC1 is correlated with curve number (*CN*) and VLUCS, and PC2 is correlated with flow velocity (*V*) and flood extension (*A*).

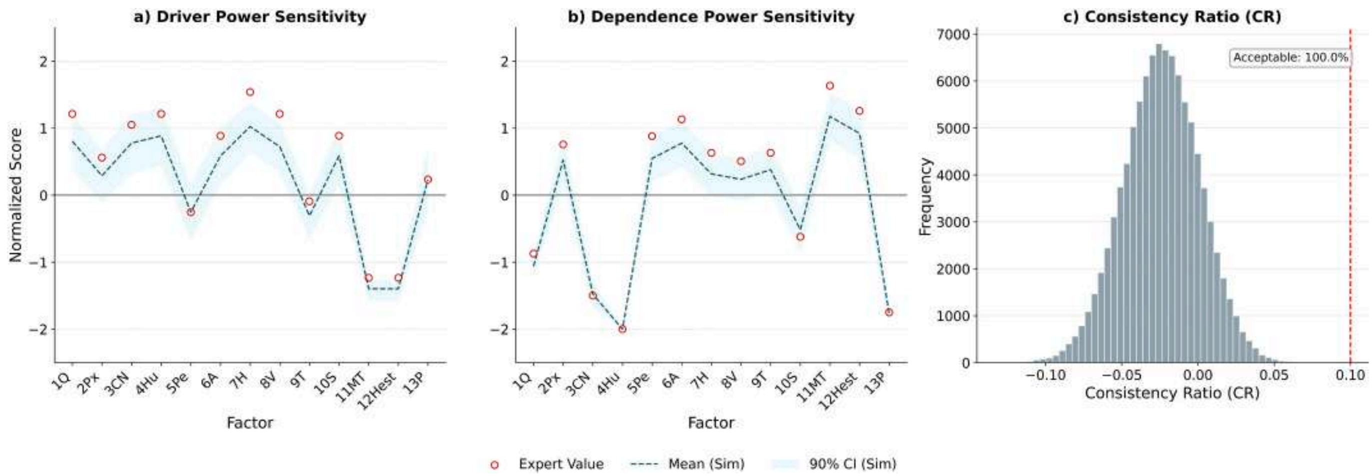


**Fig. 8.** Evaluation of expert judgment uncertainty using a Monte Carlo simulation. a) Driver values; b) Dependency values; c) Consistency ratio histogram.

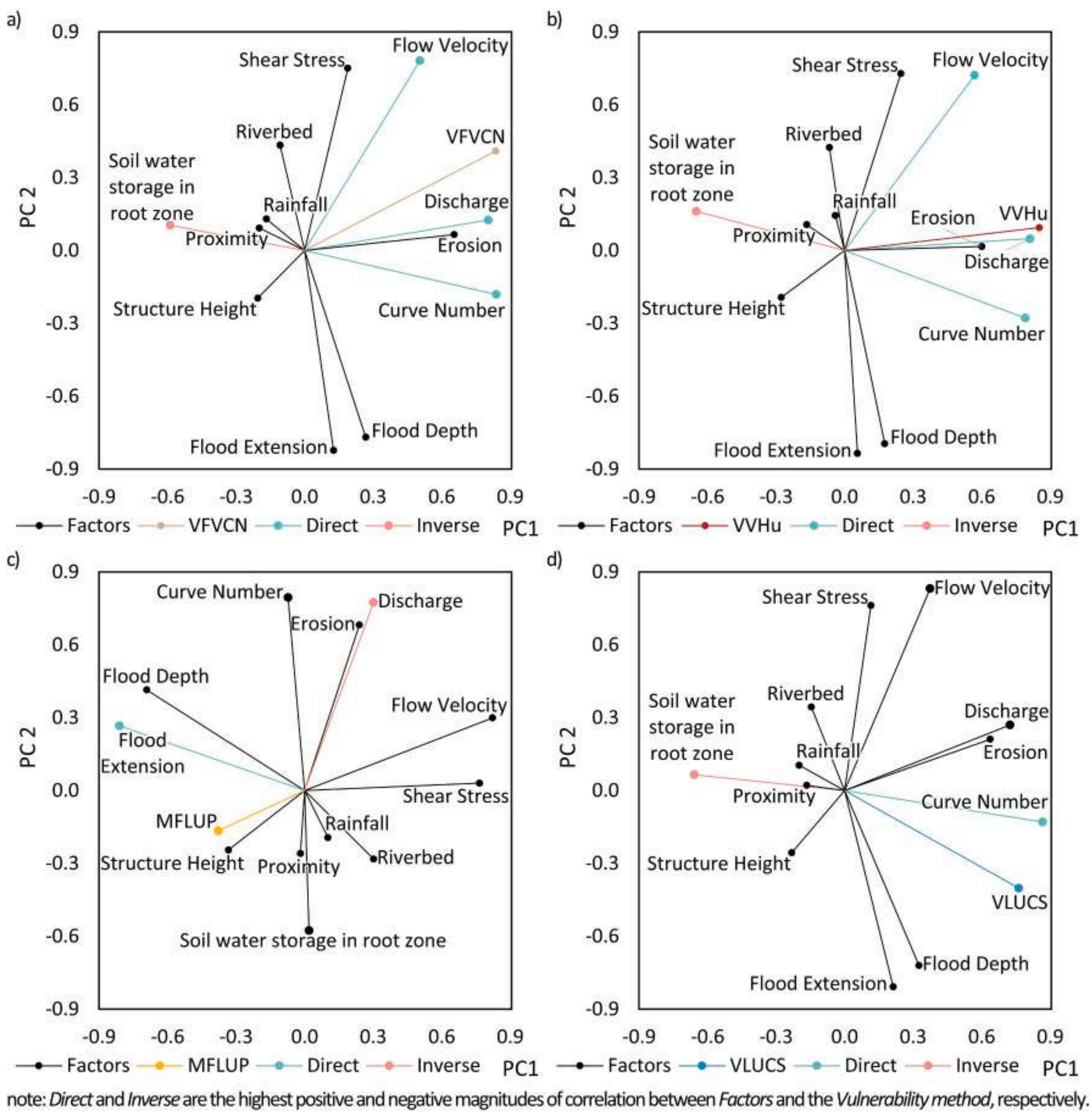


**Fig. 9.** Principal Components Analysis for vulnerability factors according to the following methods: (a) VFVCN; (b) VVHu; (c) MFLUP; (d) VLUCS.

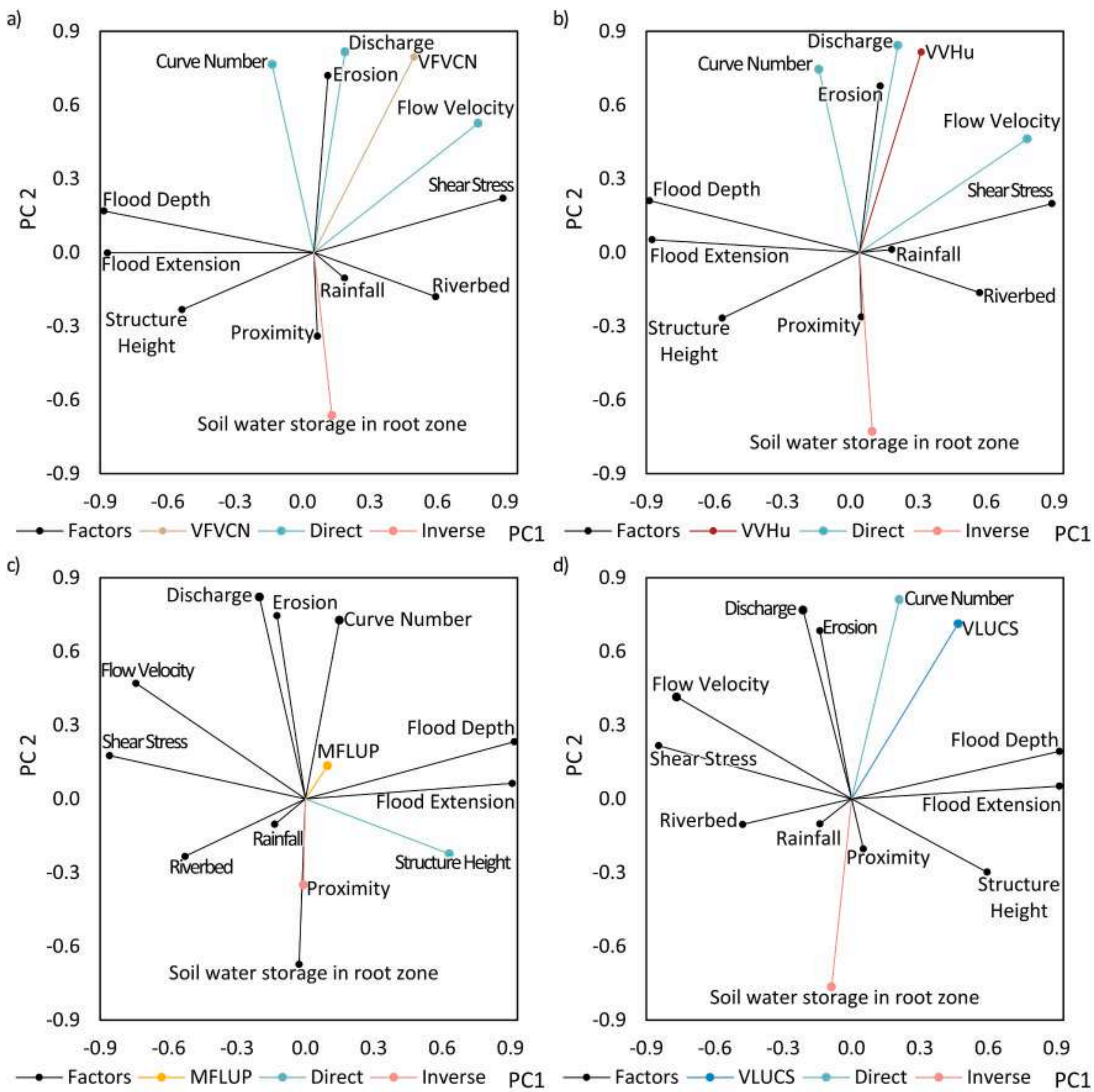


note: *Direct* and *Inverse* are the highest positive and negative magnitudes of correlation between *Factors* and the *Vulnerability method*, respectively.

**Fig. 10.** Retaining Walls PCA for vulnerability methods and factors: (a) VFVCN; (b) VVHu; (c) MFLUP; (d) VLUCS.

The correlations results between the vulnerability methods and factors selected in this study indicated that VFVCN had a positive correlation with values ranging from 0.67 to 0.78 for the following factors: discharge (*Q*), curve number (*CN*), and flow velocity (*V*), indicating that physical vulnerability increases with increasing magnitude of these factors (Fig. 9a). Similarly, the VVHu method showed a positive correlation with flow velocity (*V*), discharge (*Q*), and curve number (*CN*), with values ranging from 0.56 to 0.62 (Fig. 9b). In turn, MFLUP has a positive correlation with structure height (*Hest*) with a value of 0.41, that is, the vulnerability according to this method increases when the structure is submerged by water, or is close to being so (Fig. 9c). Finally, VLUCS had a positive correlation of 0.77 with curve number (*CN*), that is, the vulnerability increases when the soil cover increases its impermeability (Fig. 9d).

Furthermore, the VFVCN, VVHu, and VLUCS methods exhibited the strongest negative correlation with soil water storage in the root zone ($H_u$) factor with values of −0.42, −0.62, and − 0.61, respectively, and a positive relationship with curve number of 0.70, 0.63, and 0.78, respectively. That is, physical vulnerability decreases as soil storage and infiltration capacity increase. In addition the analysis was performed considering the type of structure, which were 9 retaining walls, and 13 bridges (Fig. 10 and Fig. 11, respectively), finding that the vulnerability in retaining walls presents a positive correlation with discharge (*Q*), and curve number (*CN*), and a negative relationship with soil water storage in the root zone ($H_u$), according to the results obtained with the VFVCN (Fig. 10a) and VVHu (Fig. 10b) methods. In this sense, correlations with MFLUP were not very significant (Fig. 7c), while with VLUCS, a positive correlation was identified with curve number (*CN*), and a negative one was registered with soil water storage in the root zone ($H_u$) (Fig. 10d). Likewise, vulnerability in bridges showed a positive correlation with flow velocity (*V*), discharge (*Q*), and curve number (*CN*), according to the results obtained with VFVCN (Fig. 11a) and VVHu (Fig. 11b). Results obtained with MFLUP showed a positive correlation with shear stress (*T*) and proximity (*Px*) (Fig. 11c), while physical vulnerability obtained with VLUCS had a positive correlation with discharge (*Q*) and curve number (*CN*) (Fig. 11d).

### 3.5. Correlation analysis with CATPCA

For this analysis, the physical vulnerability values obtained using each of the methods described in section 2.4 were reclassified into three categorical variables: low, medium, and high. Dimensionality reduction

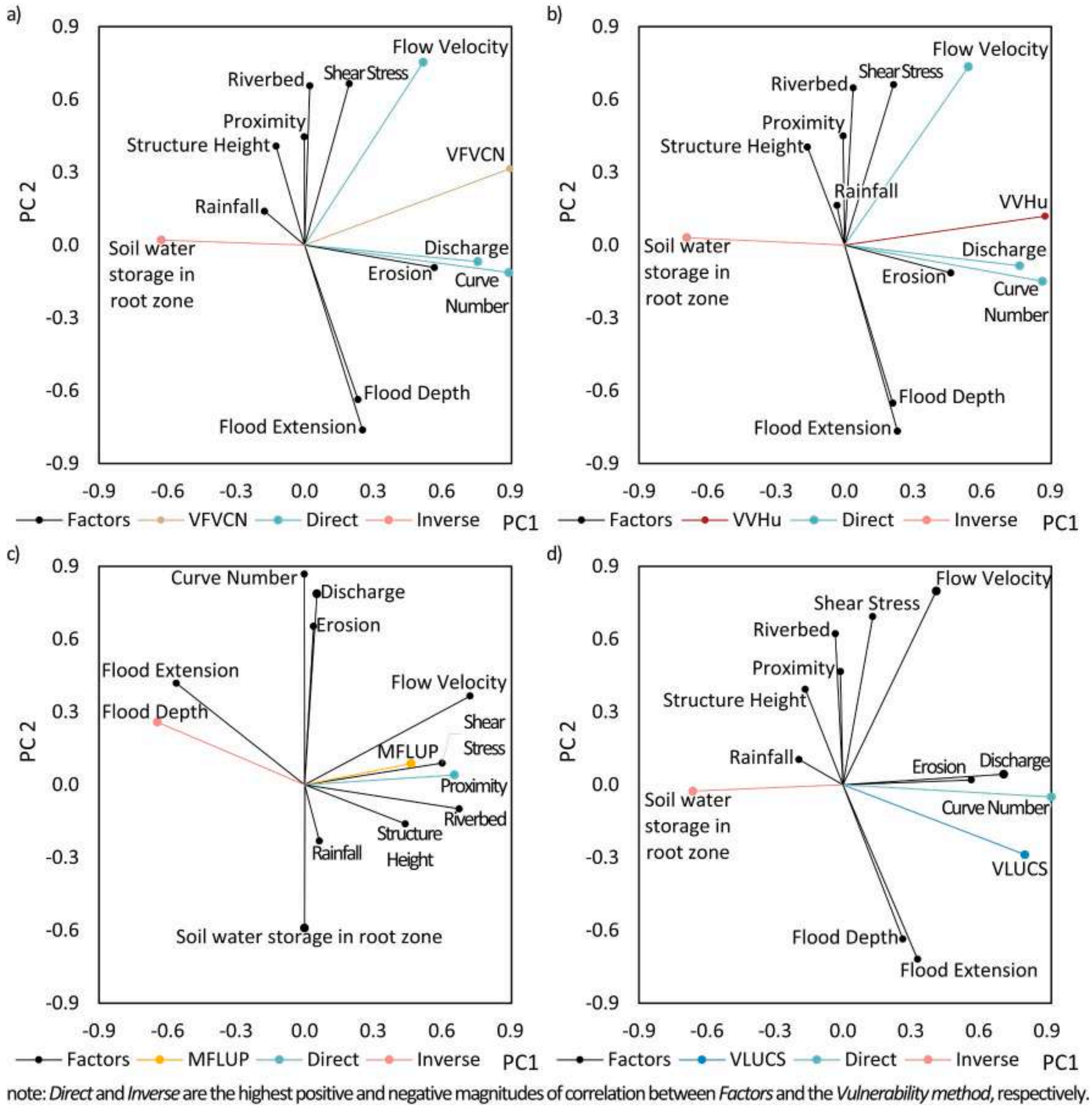


**Fig. 11.** Bridges PCA for vulnerability methods and factors: (a) VFVCN; (b) VVHu; (c) MFLUP; (d) VLUCS.

with numerical and categorical factors was performed by selecting the first two principal components (PC1 and PC2) using CATPCA [26]. In Fig. 12a, the first component is highly correlated with flood extension (*A*), flow velocity (*V*), and flood depth (*H*), and the second component is strongly correlated with curve number (*CN*) and discharge (*Q*). For Fig. 10b, PC1 is strongly correlated with flood extension (*A*) and flood depth (*H*), and PC2 is highly correlated with discharge (*Q*) and curve number (*CN*). Likewise, in Fig. 12c, PC1 is mainly correlated with flood extension (*A*), flood depth (*H*), and flow velocity (*V*), and PC2 is mostly correlated with discharge (*Q*) and potential erosion (*Ep*). Finally, Fig. 12d shows that PC1 is correlated with flood extension (*A*), flood velocity (*V*), and flood depth (*H*), and PC2 is correlated with curve number (*CN*) and discharge (*Q*). On the other hand, the material type (*MT*) factor showed low component loading for PC1 and PC2 and weak correlation among vulnerability methods (Fig. 12). The correlation results between the vulnerability methods and factors selected in this study revealed that, for the VFVCN method, high vulnerability correlates with flow velocity (*V*), discharge (*Q*), and curve number (*CN*). Low vulnerability was positively related to soil water storage in the root zone ($H_u$). That is, low vulnerability is associated with high static storage and infiltration capacity (Fig. 10a). The same is true for physical vulnerability obtained with VVHu (Fig. 12b).

Results obtained with MFLUP allowed identifying a relationship between high physical vulnerability and discharge (*Q*), while low vulnerability presented a negative correlation with proximity (*Px*). Therefore, shorter distances between the structure and the water table are associated with greater physical vulnerability of the exposed structures (Fig. 12c).

Finally, the vulnerability assessed with VLUCS showed a positive relationship between curve number (***CN***) and discharge (***Q***) with high vulnerability. In contrast, a low vulnerability was related to soil water storage in the root zone ($\boldsymbol{H_u}$) (Fig. 12d). Likewise, depending on the type of structure, high vulnerability in retaining walls was mainly related to discharge, according to the results obtained with VFVCN (Fig. 13a), VVHu (Fig. 13b), and MFLUP (Fig. 13c). Furthermore, the curve number (***CN***) was a relevant factor when vulnerability was assessed with VLUCS (Fig. 13d).

At the same time, low vulnerability was positively related to soil water storage in the root zone, according to results obtained with VFVCN (Fig. 13a), VVHu (Fig. 13b), and VLUCS (Fig. 13d). In turn, a positive correlation was found between high vulnerability in bridges, mainly with the curve number (***CN***) variable, according to the VFVCN

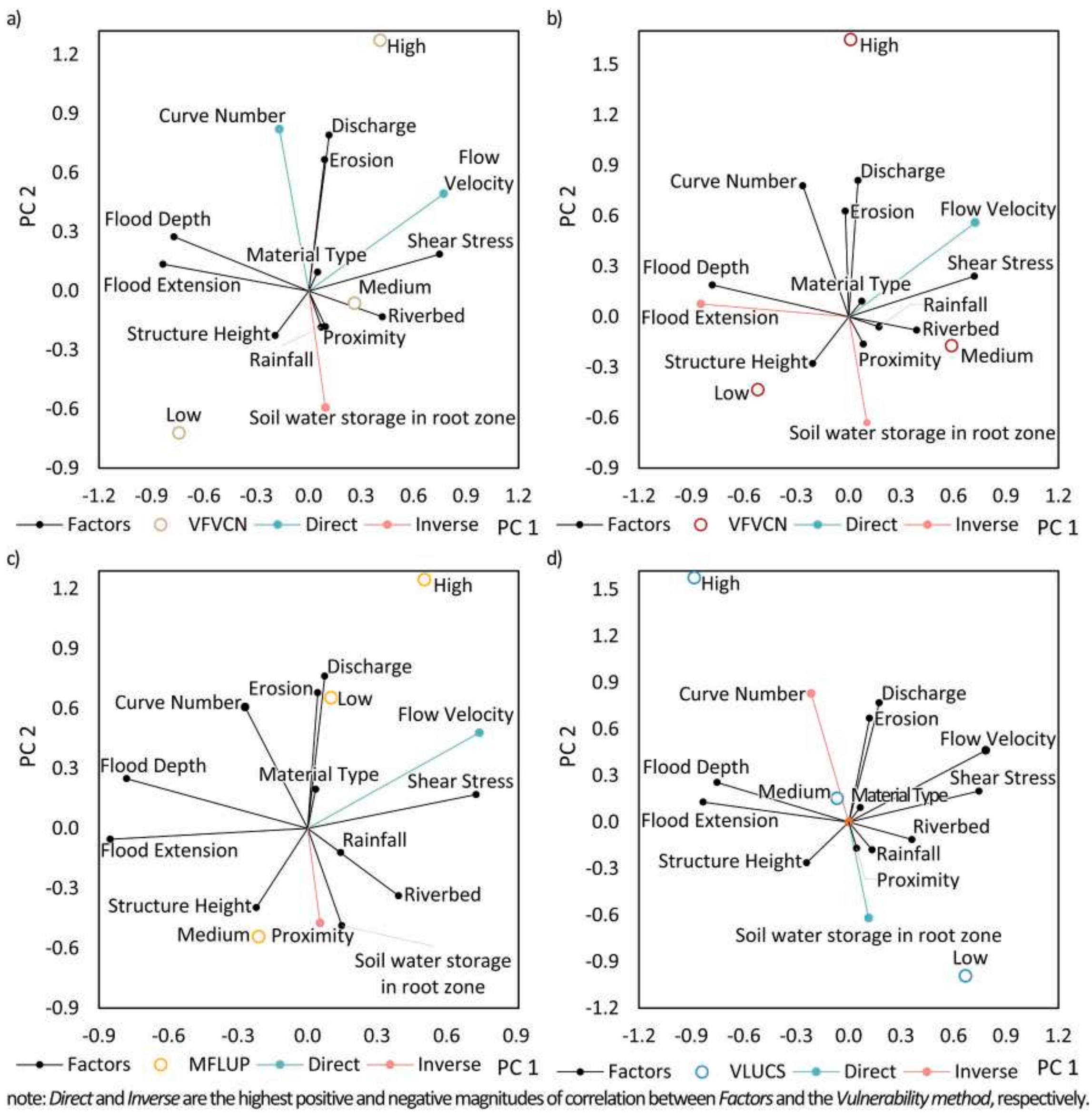


**Fig. 12.** CATPCA for vulnerability methods and factors: (a) VFVCN; (b) VVHu; (c) MFLUP; (d) VLUCS.

(Fig. 14a), VVHu (Fig. 14b), and VLUCS (Fig. 14d) methods. In this study, no bridge obtained a high vulnerability when evaluated with MFLUP (Fig. 14c). Thus, low vulnerability in bridges was related to the soil water storage in the root zone variable, when estimated with the VFVCN (Fig. 14a), VVHu (Fig. 14b), and VLUCS (Fig. 14d) methods. At the same time, with MFLUP, this relationship was registered with the material type (Fig. 14c).

### 3.6. Comparative synthesis through spearman's rank correlation

Results obtained with MICMAC are based on influence scores or expert intuition, while PCA and CATPCA produce component loadings through statistical analysis, which involves analyzing non-commutative values on different scales. However, it was possible to convert the results into ordinal ranges using Spearman's rank correlation coefficient (ρ) analysis to determine the level of monotony between the methods used to identify key factors. Based on the results reported in Table 6, the values of ρ were estimated in pairs: i) for MICMAC vs. PCA (Structural analysis vs. Linear variance) was $\rho = 0.599$, and the $p$-value was 0.031; ii) MICMAC vs. CATPCA (Structural analysis vs. Non-linear variance) $\rho = 0.604$ with a p-value of 0.029, and iii) PCA vs. CATPCA (Linear vs. Non-linear data structure) comparison was $\rho = 0.764$ and $p = 0.002$. This indicates moderate convergence among the key factors obtained with MICMAC in comparison with PCA, and CATPCA, while strong convergence was identified between PCA and CATPCA, where $p$-values $<0.05$ were considered statistically significant. This statistical convergence validates the selection of the key factors $4H_u$, $3CN$, $1Q$, and $8V$ (Table 6) identified between PCA and CATPCA, indicating that they correspond to statistically robust variables, such the MICMAC confirms these variables causally through expert evaluation, even though the driver values show low variance compared to the dataset used for the PCA.

## 4. Discussion

Table 6 contains the summary of the main results obtained through MICMAC, PCA, and CATPCA. Further, the four variables identified as most influential in the expert judgment align closely with the results obtained with PCA and CATPCA. Based on the above, the most relevant factors associated with the physical vulnerability of structures exposed to flooding were soil water storage in the root zone, curve number, discharge and flow velocity, all of which are highly related to

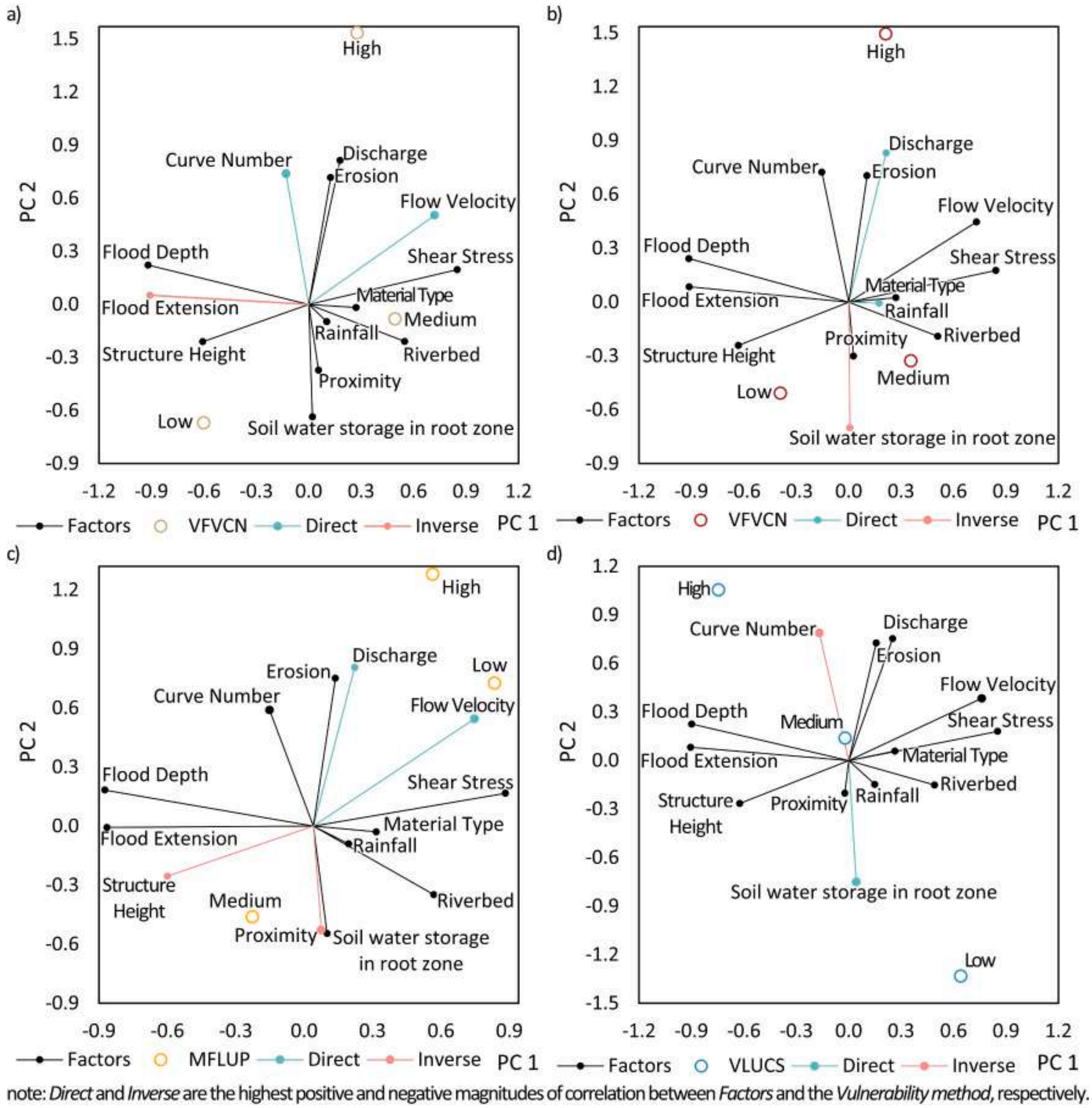


**Fig. 13.** Retaining Walls CATPCA for vulnerability methods and factors: (a) VFVCN; (b) VVHu; (c) MFLUP; (d) VLUCS.

precipitation. In this sense, soil water storage in the root zone reflects a characteristic of the hydraulic properties of the soil; the curve number represents the permeability characteristics of the soil cover; and discharge and flow velocity represent the drainage network or the evacuation of surface runoff. Thus, according to the MICMAC results, these factors showed less dependence and greater influence, and therefore, the highest magnitude of the drive values classify them as driving factors. In turn, although the flood depth factor has a drive value of 0.811, it shows a positive dependence and is not considered a key factor (Fig. 7); it is represented in green shading in Table 6. In turn, based on the correlation values obtained from the PCA for each factor in the correlation matrix, it can be observed that the physical vulnerability of structures exposed to flooding is positively correlated with the discharge and curve number factors. Likewise, the correlation matrix indicates that the factors soil water storage in the root zone, curve number, discharge, and flow velocity show correlations of $r > 0.5$ and $r < -0.5$, and therefore, are considered key factors in the evaluation of the physical vulnerability of structures exposed to flooding with the VFVCN, VVHu, and VLUCS methods. In contrast, the correlations obtained with the MFLUP method are inconclusive. This is probably because its formulation focuses primarily on the geometry of the exposed structures and does not include variables associated with land-use change. Moreover, results obtained with CATPCA were considered to be correlations with $r > 0.25$ or $r < -0.25$, and a coincidence was found between the results obtained with MICMAC and PCA. So, the high physical vulnerability of structures exposed to flooding is usually associated with high curve number and discharge values, while low physical vulnerability tends to be associated with increased soil infiltration capacity. This result is consistent with that reported by Nkeki et al. [59], who found that factors such as land use, runoff, and soil type exacerbate flood hazards by influencing soil infiltration capacity, thereby altering the rate of water infiltration into the soil and increasing surface runoff. Similarly, Narendra et al. [55] reported that geomorphometric variables, soil permeability, and infiltration capacity are inversely related to runoff production and the capacity to generate floods in watersheds. According to the expert judgment analysis using MICMAC, coincidences in the determination of those factors were identified with a high index of motricity in vulnerability. Thus, vulnerability calculated with VFVCN and VVHu showed a significant positive relationship with the velocity factor, consistent with that reported by Deschamps et al. [98], who found that a group of experts ranked flow velocity as the second most influential factor in flood damage. It has also been reported that flood

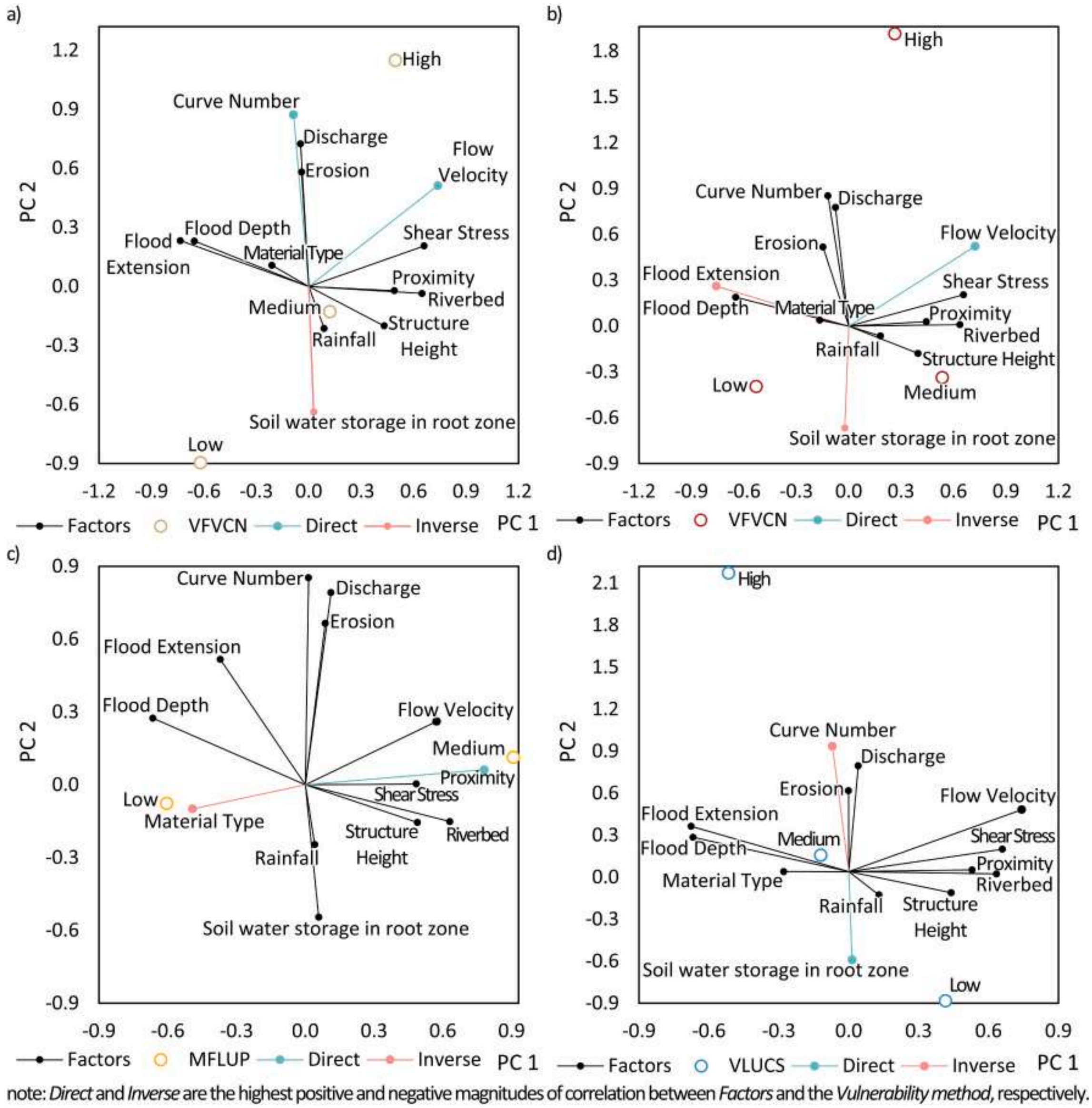


**Fig. 14.** Bridges CATPCA for vulnerability methods and factors: (a) VFVCN; (b) VVHu; (c) MFLUP; (d) VLUCS.

depth is the factor that contributes most to the degree of loss due to flooding [36] and the second factor contributing most to determining the flood hazard level [54].

On the other hand, the vulnerability correlation matrix values obtained with the MFLUP method did not obtain conclusive correlations in this analysis that would allow finding coincidence of key factors determined with MICMAC, PCA and CATPCA (Table 6), which can be attributed to the fact that the variables that define the method focus on the geometry of structures, their proximity to the stream and do not incorporate processes related to land use or its hydraulic properties.

Studies on flood drivers and vulnerability in mountain basins classify exposure and susceptibility of structures as key factors (e.g., [99]). However, in this study, land use change, infiltration capacity, and soil hydraulic properties have been evaluated as determining factors, given their high influence on runoff generation, as reported by Hyder Soomro et al. [50], Gebremichael et al. [100] and Xu et al. [101], as well as flow velocity and discharge due to their interaction with structures. This contrasts with studies conducted in urban areas, which emphasize factors such as rainfall and the physical characteristics of structures [10], such as height and building location, design specifications, surrounding vegetation cover [102], and water table depth [103].

Finally, research reports that land-use change can increase or attenuate peak flows as a non-structural measure to address the effects of flooding (e.g., [104,105]). Likewise, vegetation cover distribution is crucial for soil water retention, flood formation [30,106], and the aggravation of flood hazard [107,108]. Afforestation, in particular, contributes to reducing flood risk and brings ecological and socioeconomic benefits to mountain watersheds, thus aligning with the concept of nature-based solutions [18]. This can be integrated with land-use planning and policies to improve the resilience of structures exposed to flooding [109]. The results of this study indicate a high degree of influence of soil water infiltration and storage capacity on the physical vulnerability of structures exposed to flooding. This is consistent with the findings of López and Francés [110] and Visessri and Ekkawatpanit [111] in their assessments of the effects of LUC and climate change on hydrological systems. Therefore, the key factors identified in this study may be useful for land-use planning and the implementation of non-structural flood-control measures.

## 5. Limitations and scope

The proposed methodology was designed to identify key factors for

**Table 6**
Results obtained from MICMAC, PCA, and CATPCA.

| Variable | Description | MIC MAC Results | | PCA Results Vulnerability Correlation Matrix | | | | CATPCA Results Vulnerability Correlation Matrix | | | |
|---|---|---|---|---|---|---|---|---|---|---|---|
| | | Driver value | Dependence | VVHu | VFVCN | VLUCS | MFLUP | VVHu | VFVCN | VLUCS | MFLUP |
| 4$H_u$ | Soil water storage in root zone | 1.375 | -1.368 | -0.622 | -0.418 | -0.609 | -0.090 | -0.252 | -0.333 | 0.509 | -0.118 |
| 3$CN$ | Curve number | 0.857 | -1.115 | 0.627 | 0.704 | 0.780 | 0.046 | 0.034 | 0.539 | -0.721 | 0.013 |
| 7$H$ | Flood depth | 0.811 | 0.058 | 0.053 | -0.070 | 0.432 | 0.073 | -0.215 | -0.185 | -0.416 | 0.041 |
| 1$Q$ | Discharge | 0.704 | -1.280 | 0.615 | 0.672 | 0.244 | -0.231 | 0.061 | 0.434 | -0.315 | 0.288 |
| 8$V$ | Flow velocity | 0.550 | -0.001 | 0.559 | 0.777 | -0.059 | -0.091 | 0.290 | 0.618 | 0.026 | 0.346 |
| 10$S$ | Riverbed | 0.529 | -0.327 | 0.064 | 0.175 | -0.133 | 0.167 | 0.006 | 0.144 | 0.121 | -0.325 |
| 6$A$ | Flood area | 0.388 | 0.717 | 0.011 | -0.203 | 0.410 | 0.291 | -0.300 | -0.312 | -0.402 | -0.352 |
| 13$P$ | Precipitation | 0.013 | -1.216 | 0.180 | -0.071 | -0.202 | -0.076 | 0.168 | -0.264 | 0.212 | 0.032 |
| 2$Px$ | Proximity | -0.137 | 0.945 | -0.064 | -0.108 | -0.045 | 0.228 | -0.019 | -0.026 | 0.060 | -0.670 |
| 5$Ep$ | Erosion | -0.773 | 0.469 | 0.267 | 0.429 | 0.266 | -0.166 | -0.177 | 0.389 | -0.349 | 0.282 |
| 9$T$ | Shear stress | -0.778 | 0.345 | 0.195 | 0.421 | -0.181 | -0.221 | 0.205 | 0.400 | 0.144 | 0.087 |
| 12$Hest$ | Structure height | -1.724 | 1.195 | -0.222 | -0.133 | -0.078 | 0.414 | -0.078 | -0.087 | 0.063 | -0.400 |
| 11$TM$ | Material type | -1.815 | 1.577 | | | | | 0.164 | 0.109 | 0.008 | 0.081 |

The key factors identified by each method are highlighted in green.

assessing the physical vulnerability of structures exposed to flooding at the basin scale in non-urban areas under changing land-use scenarios. Therefore, the vulnerability of structures such as bridges and retaining walls located along the analyzed river reach was analyzed. These structures serve to protect and stabilize road infrastructure, human settlements in riparian zones, drinking water supply structures, and agricultural areas. This is aligned with the goals established in the Framework for Disaster Risk Reduction 2015–2030 [37].

In this sense, the availability of information may limit the implementation of the proposed methodology. Therefore, identifying key factors in assessing physical vulnerability can be highly valuable, as it helps prioritize resources for flood studies in areas with limited information and resources.

In this context, the reported results correspond to the analysis conducted in the Combeima River basin, located in the Andes mountain range in Colombia, where system modeling was conducted using hydroclimatological series and land use maps, allowing for the analysis of the hydrological cycle in the study area over a 53-year period with daily temporal resolution and a grid resolution of 90 × 90 m. The hydraulic model described the channel geometry using 150 cross sections measured along the analyzed river reach. In this sense, the availability of information may limit the implementation of the proposed methodology. Thus, identifying key factors in assessing physical vulnerability can be invaluable, as it can help prioritize resources for flood studies in areas with limited information and resources [112]. Therefore, the proposed methodology could be implemented under equivalent morphological and climatological conditions. In this sense, other researchers are encouraged to conduct similar studies in watersheds with diverse relief and latitude, which could lead to the establishment of criteria for the broad transferability of the methodology. Likewise, research evaluating the contributions of runoff in shaping land-use and climate change environments is necessary to establish structures that protect people and their livelihoods, contributing to community resilience.

According to Rangasamy and Yang [34], stakeholder representation imbalance might not fully represent the phenomenon; likewise, MICMAC analyses are based on perceptions and interpretations that may have inherent constraints in capturing the complexity of factor interactions. Therefore, in this study, the combined application of MICMAC, PCA, and CATPCA offers a complementary approach to analyzing results across different dimensions, which can complicate their statistical comparison. In this sense, the need to develop research aimed at establishing the convergence or divergence between statistical and subjective methods is identified.

Finally, discharge and flow velocity have been widely used in the design of early warning systems for floods. Thus, this study identified a strong influence of variables related to land-use change, which could be relevant for the design of prediction and early warning systems that involve monitoring soil moisture and water storage at the watershed scale.

## 6. Conclusions

In this study, through distributed hydrological and hydraulic modeling and the implementation of MICMAC, APC, and CATPCA, it was possible to identify the most influential factors affecting the physical vulnerability of structures exposed to flooding along the Combeima River. The results demonstrated that soil water storage in the root zone and curve number are the crucial factors that determine the level of physical vulnerability to flooding in the analyzed structures. A high infiltration capacity in the root zone is associated with low levels of physical vulnerability of structures exposed to flooding, whereas soil cover configurations with greater impermeability tend to produce high levels of vulnerability in the analyzed structures. Likewise, the MICMAC analysis showed that factors such as discharge, riverbed, flood depth, and flow velocity have a high motricity index, leading to higher levels of physical vulnerability of structures. Similarly, results from PCA and CATPCA indicate that the flow velocity factor shows a strong positive correlation with the physical vulnerability of structures exposed to flooding.

This study combined expert judgment with multivariate statistical analysis, finding moderate to strong convergence between methods. This approach facilitated the identification of key factors that determine the level of physical vulnerability of structures exposed to flooding, which can be useful for planning and flood risk management. Therefore, the complementarity identified between methods reinforces the need to implement the hybrid approach proposed in this study. In this case, PCA and CATPCA evaluated the central characteristics of the data structure to identify the variance of nonlinear processes, while their causes can be incorporated using MICMAC.

## CRediT authorship contribution statement

**Yelena Hernández-Atencia:** Writing – original draft, Methodology, Investigation, Formal analysis, Data curation. **Juanchito Cutupey-Márquez:** Writing – original draft, Validation, Methodology, Data curation. **Isabel Rojas:** Validation, Formal analysis, Data curation. **Didier Lizcano:** Validation, Formal analysis, Data curation. **Jader Muñoz-Ramos:** Writing – review & editing, Methodology, Conceptualization. **Luis E. Peña:** Writing – original draft, Validation, Methodology, Investigation, Formal analysis, Conceptualization.

## Funding

This work was funded by the doctoral fellowship program of Universidad Cooperativa de Colombia [Res 877/16-12-2014] and Universidad de Ibagué [Project 19-500-INT].

## Declaration of competing interest

The authors declare that they have no known competing financial interests or personal relationships that could have appeared to influence the work reported in this paper.

## Acknowledgments

The authors would like to thank Drs. Miguel Barrios and Jorge Mario Vera of Universidad del Tolima, Alberto Nuñez-Tello of the Colombian Geological Survey, and Miguel Thomas of the Interinstitutional Committee for Environmental Education, who participated in the expert judgment assessment. Many thanks to Ms. Cristina Rojas, Ibagué Police Department, Department of Topography of the Faculty of Technology of Universidad del Tolima, and the Department of Civil Engineering of Universidad de Ibagué, for their support in conducting bathymetry surveys of the Combeima River used in this study.

## Data availability

Data will be made available upon request to the corresponding author.

## References

[1] Calvin K, Dasgupta D, Krinner G, Mukherji A, Thorne PW, Trisos C, et al. IPCC, 2023: climate change 2023: synthesis report. In: Core Writing Team, Lee H, Romero J, editors. Contribution of Working Groups I, II and III to the Sixth Assessment Report of the Intergovernmental Panel on Climate Change. Geneva, Switzerland: Intergovernmental Panel on Climate Change (IPCC); 2023.

[2] WMO. Economic costs of weather-related disasters soars but early warnings save lives. 2023.

[3] WMO. Status of mortality and economic losses [WWW document]. World Meteorol. Organ; 2025. URL, https://storymaps.arcgis.com/stories/8df884dbd4e849c89d4b1128fa5dc1d6 (accessed 8.27.25).

[4] Delforge D, Below R, Lanfredi Sofia C, Tonnelier M, van Loenhout JAF, Speybroeck N. EM-DAT: the emergency events database [WWW Document]. Cent. Res. Epidemiol. Disasters; 2025. https://doi.org/10.21203/rs.3.rs-3807553/v1.

[5] Jiménez-U M, Peña LE, López J. Non-stationary analysis for road drainage design under land-use and climate change scenarios. Heliyon 2022;8. https://doi.org/10.1016/j.heliyon.2022.e08942. 1–12.

[6] Hernández-Atencia Y, Peña LE, Muñoz-Ramos J, Rojas I, Álvarez A. Use of soil infiltration capacity and stream flow velocity to estimate physical flood vulnerability under land-use change scenarios. Water (Switzerland) 2023;15:1–16. https://doi.org/10.3390/w15061214.

[7] Romshoo SA, Altaf S. Assessing flood vulnerability in the upper Jhelum Basin using a geospatial modelling approach. Geomat Nat Haz Risk 2025;16:2435507. https://doi.org/10.1080/19475705.2024.2435507.

[8] Kaoje IU, Zulkarnain M, Rahman A, Idris NH, Razak KA, Nurul W, et al. Physical flood vulnerability assessment using geospatial indicator-based approach and participatory analytical. Water 2021;13:1–22.

[9] Papathoma-Köhle M, Kappes M, Keiler M, Glade T. Physical vulnerability assessment for alpine hazards: state of the art and future needs. Nat Hazards 2011;58:645–80. https://doi.org/10.1007/s11069-010-9632-4.

[10] Papathoma-Köhle M, Schlögl M, Dosser L, Roesch F, Borga M, Erlicher M, et al. Physical vulnerability to dynamic flooding: vulnerability curves and vulnerability indices. J Hydrol 2022;607. https://doi.org/10.1016/j.jhydrol.2022.127501.

[11] Dell'Agnese A, Mazzorana B, Comiti F, Von Maravic P, D'agostino V. Assessing the physical vulnerability of check dams through an empirical damage index. J Agric Eng 2013;43:2. https://doi.org/10.4081/jae.2013.e2.

[12] Caldas AM, Pissarra TCT, Costa RCA, Neto FCR, Zanata M, da Parahyba RBV, et al. Flood vulnerability, environmental land use conflicts, and conservation of soil and water: a study in the Batatais SP municipality, Brazil. Water (Switzerland) 2018;10. https://doi.org/10.3390/w10101357.

[13] Liu J, Shi Z, Wang D. Measuring and mapping the flood vulnerability based on land-use patterns: a case study of Beijing. China Nat Hazards 2016;83:1545–65. https://doi.org/10.1007/s11069-016-2375-0.

[14] Bhat MS, Khan AA, Akbar M, Mir S. Disaster-development interface and its impact on emerging vulnerability scenario in Ladakh region of northwestern Himalayas. J Environ Stud Sci 2023;13:253–70. https://doi.org/10.1007/s13412-023-00818-9.

[15] Tascón-González L, Ferrer-Julià M, García-Meléndez E. Methodological approach for mapping the flood physical vulnerability index with geographical open-source data: an example in a small-middle city (Ponferrada, Spain). Nat Hazards 2024;120:4053–81. https://doi.org/10.1007/s11069-023-06370-7.

[16] Karagiorgos K, Thaler T, Heiser M, Hübl J, Fuchs S. Integrated flash flood vulnerability assessment: insights from East Attica, Greece. J Hydrol 2016;541:553–62. https://doi.org/10.1016/j.jhydrol.2016.02.052.

[17] Lei Y, Finlayson M, Thwaites R, Shi G. Migration drivers in mountain regions in the context of climate change: a case study in Shangnan County of China. Chinese J Popul Resour Environ 2013;11:200–9. https://doi.org/10.1080/10042857.2013.818438.

[18] Conitz F, Zingraff-Hamed A, Lupp G, Pauleit S. Non-structural flood management in european rural mountain areas—are scientists supporting implementation? Hydrology 2021;8:1–37. https://doi.org/10.3390/hydrology8040167.

[19] Stoffel M, Wyżga B, Marston RA. Floods in mountain environments: a synthesis. Geomorphology 2016;272:1–9. https://doi.org/10.1016/j.geomorph.2016.07.008.

[20] Li K, Guo L, Wang G, Gao J, Ma J, Li J, et al. A novel hybrid framework of high-resolution flood susceptibility mapping in ungauged mountainous regions. Weather Clim Extrem 2025;50:1–15. https://doi.org/10.1016/j.wace.2025.100822.

[21] Yves T, Villarini G, El Khalki EM, Gründemann G, Hughes D. Evaluation of the drivers responsible for flooding in Africa. Water Resour Res 2021;57:1–14. https://doi.org/10.1029/2021WR029595.

[22] Mazzorana B, Comiti F, Scherer C, Fuchs S. Developing consistent scenarios to assess flood hazards in mountain streams. J Environ Manage 2012;94:112–24. https://doi.org/10.1016/j.jenvman.2011.06.030.

[23] Winsemius HC, Aerts JCJH, Van Beek LPH, Bierkens MFP, Bouwman A, Jongman B, et al. Global drivers of future river flood risk. Nat Clim Chang 2016;6:381–5. https://doi.org/10.1038/nclimate2893.

[24] Ariyani D, Purwanto MYJ, Sunarti E, Perdinan. Contributing factor influencing flood disaster using MICMAC (Ciliwung watershed case study). J Pengelolaan Sumberd Alam dan Lingkung 2022;12:268–80. https://doi.org/10.29244/jpsl.12.2.268-280.

[25] Sharma S, Sharma V. Identification and prioritization of flood conditioning factors using ISM and MICMAC technique. Int J Innov Technol Explor Eng 2019;8:143–8. https://doi.org/10.35940/ijitee.I1121.0789S419.

[26] Martins B, Nunes A. Exploring flash flood risk perception using PCA analysis: the case of Mindelo, S. Vicente (Cape Verde). Geogr J 2020;186:375–89. https://doi.org/10.1111/GEOJ.12357.

[27] Hasanuzzaman M, Bera B, Islam A, Shit PK. Exploring GIS-based modeling for assessing social vulnerability to Ganga Riverbank erosion, India. Nat Hazards Res 2024. https://doi.org/10.1016/j.nhres.2024.08.001.

[28] Islam MT, Meng Q. Spatial analysis of socio-economic and demographic factors influencing urban flood vulnerability. J Urban Manag 2024;13:437–55. https://doi.org/10.1016/j.jum.2024.06.001.

[29] Dell'Agnese A, Mazzorana B, Comiti F, Von Maravic P, D'Agostino V. Assessing the physical vulnerability of check dams through an empirical damage index. J Agric Eng 2013;44:9–16. https://doi.org/10.4081/jae.2013.e2.

[30] Karmaoui A, Zerouali S, Ayt H, Ashfaq O, Shah A. A new mountain flood vulnerability index (MFVI) for the assessment of flood vulnerability. Sustain Water Resour Manag 2021;7:1–13. https://doi.org/10.1007/s40899-021-00575-z.

[31] Doorga J, Magerl L, Bunwaree P, Zhao J, Watkins S, Staub C, et al. GIS-based multi-criteria modelling of flood risk susceptibility in Port Louis, Mauritius: towards resilient flood management. Int J Disast Risk Reduct 2022;67. https://doi.org/10.1016/j.ijdrr.2021.102683.

[32] Rogelis M, Werner M, Obregón N, Wright N. Regional prioritisation of flood risk in mountainous areas. Nat Hazards Earth Syst Sci 2016;16:833–53. https://doi.org/10.5194/nhess-16-833-2016.

[33] Rahayu HP, Zulfa KI, Nurhasanah D, Haigh R, Amaratunga D, Wahdiny II. Unveiling transboundary challenges in river flood risk management: learning from the Ciliwung River basin. Nat Hazards Earth Syst Sci 2024;24:2045–64. https://doi.org/10.5194/nhess-24-2045-2024.

[34] Rangasamy V, Yang J Bin. Interpreting crucial barriers to advancing prefabricated construction: an empirical study in Taiwan using ISM-MICMAC approach. J Clean Prod 2025;489:144702. https://doi.org/10.1016/j.jclepro.2025.144702.

[35] Pathak S, Panta HK, Bhandari T, Paudel KP. Flood vulnerability and its influencing factors. Nat Hazards 2020;104:2175–96. https://doi.org/10.1007/s11069-020-04267-3.
[36] Sekajugo J, Kagoro-Rugunda G, Mutyebere R, Kabaseke C, Mubiru D, Kanyiginya V, et al. Exposure and physical vulnerability to geo-hydrological hazards in rural environments: a field-based assessment in East Africa. Int J Disast Risk Reduct 2024;102:104282. https://doi.org/10.1016/j.ijdrr.2024.104282.
[37] United Nations Office for Disaster Risk Reduction (UNDRR). Sendai framework for disaster risk reduction 2015–2030. 2015.
[38] Merz R, Bloschl G. Flood frequency hydrology : 1. Temporal, spatial, and causal expansion of information. Water Resour Res 2008;44:1–17. https://doi.org/10.1029/2007WR006744.
[39] Li Q, Tang Y, Wang S, Wu X, Luan Y. Mountain flood risk: a bibliometric exploration across three decades. Water (Switzerland) 2025;17:1–19. https://doi.org/10.3390/w17101513.
[40] Ahmed IA, Talukdar S, Waseem M, Shahfahad N, Rahman A. Multi - dimensional assessment of flood susceptibility drivers in the urban watershed of Guwahati. Acta Geophys 2025;73:5815–37. https://doi.org/10.1007/s11600-025-01666-7.
[41] Desalegn H, Mulu A. Heliyon flood vulnerability assessment using GIS at fetam watershed, Upper Abbay Basin7. Ethiopia Heliyon; 2021. p. e05865. https://doi.org/10.1016/j.heliyon.2020.e05865.
[42] Rodríguez D, Kasra C, Shahi R, Sairam N, Fischer M, Samprogna G, et al. Key drivers of flash flood damage to private households. J Flood Risk Manag 2025;18:1–22. https://doi.org/10.1111/jfr3.70088.
[43] Malinowska D, Milillo P, Blenkinsopp C, Giardina G. Global geo-hazard risk assessment of long- span bridges enhanced with InSAR availability. Nat Commun 2025;16:1–14. https://doi.org/10.1038/s41467-025-64260-x.
[44] UNDRR. Definition & classification review. Geneva: Switzerland; 2020.
[45] Builes-jaramillo A, Winson AEG, Bee E, Quirós N, Urán D, Rúa J, et al. Community-driven natural hazard and physical vulnerability assessment in a disaster-prone urban neighborhood. Nat Hazards Earth Syst Sci 2025;25:4451–73. https://doi.org/10.5194/nhess-25-4451-2025.
[46] Feloni E. Flood vulnerability assessment using a GIS-based multi-criteria approach — the case of Attica region. J Flood Risk Manag 2020;13:1–15. https://doi.org/10.1111/jfr3.12563.
[47] Khoso WA, Waseem M, Tanoli MA, Baig F. Flood risk susceptibility analysis in Larkana district Pakistan using multi criteria decision analysis and geospatial techniques. Sci Rep 2025;15:1–20.
[48] Vose D. Risk analysis: A quantitative guide. 3rd ed. Chichester, England: John Wiley & Sons; 2008.
[49] Chatziioannou I, Bakogiannis E, Kyriakidis C, Alvarez-Icaza L. A prospective study for the mitigation of the climate change effects: the case of the North Aegean region of Greece. Sustain 2020;12:1–20. https://doi.org/10.3390/su122410420.
[50] Hyder Soomro S, Wei H, Boota MW, Soomro NE Hyde, Faisal M, Nazli S, et al. River basin urban flood resilience: a multi-dimensional framework for risk mitigation to adaptive management and ecosystem protection under changing climate. Eco Inform 2025;91:103412. https://doi.org/10.1016/j.ecoinf.2025.103412.
[51] Thakur DA, Mohanty MP. Exploring the fidelity of satellite precipitation products in capturing flood risks: {A} novel framework incorporating hazard and vulnerability dimensions over a sensitive coastal multi-hazard catchment. Sci Total Environ 2024;920:170884. https://doi.org/10.1016/j.scitotenv.2024.170884.
[52] Pervaiz F, Hummel MA. Effects of climate change and urbanization on bridge flood vulnerability: a regional assessment for Harris County, Texas. Nat Hazards Rev 2023;24:1–10. https://doi.org/10.1061/nhrefo.nheng-1720.
[53] Bento AM, Gomes A, Viseu T, Couto L, Pêgo JP. Risk-based methodology for scour analysis at bridge foundations. Eng Struct 2020;223:111115. https://doi.org/10.1016/j.engstruct.2020.111115.
[54] Bunmi Mudashiru R, Sabtu N, Abdullah R, Saleh A, Abustan I. Optimality of flood influencing factors for flood hazard mapping: {An} evaluation of two multi-criteria decision-making methods. J Hydrol 2022;612:128055. https://doi.org/10.1016/j.jhydrol.2022.128055.
[55] Narendra BH, Setiawan O, Hasan RA, Siregar CA, Pratiwi Sari N, Sukmana A, et al. Flood susceptibility mapping based on watershed geomorphometric characteristics and land use/land cover on a small island. Glob J Environ Sci Manag 2024;10:301–20. https://doi.org/10.22034/gjesm.2024.01.19.
[56] Sperotto A, Torresan S, Gallina V, Coppola E, Critto A, Marcomini A. A multi-disciplinary approach to evaluate pluvial floods risk under changing climate: the case study of the municipality of Venice (Italy). Sci Total Environ 2016;562:1031–43. https://doi.org/10.1016/j.scitotenv.2016.03.150.
[57] Prokešová R, Horáčková Š, Snopková Z. Surface runoff response to long-term land use changes: {Spatial} rearrangement of runoff-generating areas reveals a shift in flash flood drivers. Sci Total Environ 2022;815:151591. https://doi.org/10.1016/j.scitotenv.2021.151591.
[58] USDA-SCS. Part 630 hydrology National Engineering Handbook Chapter 10 estimation of direct runoff from storm rainfall. National Engineering Handbook; 1972.
[59] Nkeki FN, Bello EI, Agbaje IG. Flood risk mapping and urban infrastructural susceptibility assessment using a GIS and analytic hierarchical raster fusion approach in the Ona River Basin, Nigeria. Int J Disast Risk Reduct 2022;77:103097. https://doi.org/10.1016/j.ijdrr.2022.103097.
[60] Francés F, Vélez JI, Vélez JJ. Split-parameter structure for the automatic calibration of distributed hydrological models. J Hydrol 2007;332:226–40. https://doi.org/10.1016/j.jhydrol.2006.06.032.
[61] Ghanbarian B, Hunt AG, Skaggs TH, Jarvis N. Upscaling soil saturated hydraulic conductivity from pore throat characteristics. Adv Water Resour 2017;104:105–13. https://doi.org/10.1016/j.advwatres.2017.03.016.
[62] Siswanto SY, Francés F. How land use/land cover changes can affect water, flooding and sedimentation in a tropical watershed: a case study using distributed modeling in the Upper Citarum watershed, Indonesia. Environ Earth Sci 2019;78:1–15. https://doi.org/10.1007/s12665-019-8561-0.
[63] Peña LE, Barrios M, Francés F. Flood quantiles scaling with upper soil hydraulic properties for different land uses at catchment scale. J Hydrol 2016;541:1258–72. https://doi.org/10.1016/j.jhydrol.2016.08.031.
[64] Wang J, Dai Z, Fagherazzi S, Zhang X, Liu X. Hydro-morphodynamics triggered by extreme riverine floods in a mega fluvial-tidal delta. Sci Total Environ 2022;809:152076. https://doi.org/10.1016/j.scitotenv.2021.152076.
[65] Loli M, Kefalas G, Dafis S, Mitoulis SA, Schmidt F. Bridge-specific flood risk assessment of transport networks using GIS and remotely sensed data. Sci Total Environ 2022;850:157976. https://doi.org/10.1016/j.scitotenv.2022.157976.
[66] Julien PY. Erosion and sedimentation. Cambridge: Cambridge University Press; 1995. https://doi.org/10.1017/CBO9781139174107.
[67] Renard KG, Freimund JR. Using monthly precipitation data to estimate the {R}-factor in the revised {USLE}. J Hydrol 1994;157:287–306. https://doi.org/10.1016/0022-1694(94)90110-4.
[68] Kabir SMI, Ahmari H, Dean M. Experimental study to investigate the effects of bridge geometry and flow condition on hydrodynamic forces. J Fluids Struct 2022;113:103688. https://doi.org/10.1016/j.jfluidstructs.2022.103688.
[69] Loli M, Mitoulis SA, Tsatsis A, Manousakis J, Kourkoulis R, Zekkos D. Flood characterization based on forensic analysis of bridge collapse using UAV reconnaissance and CFD simulations. Sci Total Environ 2022;822:153661. https://doi.org/10.1016/j.scitotenv.2022.153661.
[70] Alabbad Y, Mount J, Campbell AM, Demir I. Assessment of transportation system disruption and accessibility to critical amenities during flooding: {Iowa} case study. Sci Total Environ 2021;793:148476. https://doi.org/10.1016/j.scitotenv.2021.148476.
[71] Langlois BK, Marsh E, Stotland T, Simpson RB, Berry K, Carroll DA, et al. Usability of existing global and national data for flood related vulnerability assessment in {Indonesia}. Sci Total Environ 2023;873:162315. https://doi.org/10.1016/j.scitotenv.2023.162315.
[72] Shuka KAM, Wang K, Abubakar GA, Xu T. Impact of structural and non-structural measures on the risk of flash floods in arid and semi-arid regions: a case study of the Gash River, Kassala, Eastern Sudan. Sustain 2024;16. https://doi.org/10.3390/su16051752.
[73] Paul A, Biswas M. Changes in river bed terrain and its impact on flood propagation–a case study of river Jayanti, West Bengal, India. Geomat Nat Haz Risk 2019;10:1928–47. https://doi.org/10.1080/19475705.2019.1650124.
[74] Habersack H, Hein T, Stanica A, Liska I, Mair R, Jäger E, Hauer C, Bradley C. Challenges of river basin management: Current status of, and prospects for, the River Danube from a river engineering perspective. Sci. Total Environ. 2016;543:828–45. https://doi.org/10.1016/j.scitotenv.2015.10.123.
[75] Crotti G, Cigada A. Scour at river bridge piers: real-time vulnerability assessment through the continuous monitoring of a bridge over the river Po, Italy. J Civ Struct Heal Monit 2019;9:513–28. https://doi.org/10.1007/s13349-019-00348-5.
[76] Bussi G, Francés F, Montoya JJ, Julien PY. Distributed sediment yield modelling: importance of initial sediment conditions. Environ Model Software 2014;58:58–70. https://doi.org/10.1016/j.envsoft.2014.04.010.
[77] Moriasi DN, Arnold JG, Van Liew MW, Binger RL, Harmel RD, Veith TL. Model evaluation guidelines for systematic quantification of accuracy in watershed simulations. Trans ASABE 2007;50:885–900. https://doi.org/10.13031/2013.23153.
[78] U.S. Army Corps of Engineers. HEC-RAS river analysis system. 2020.
[79] Qian Q, Edwards DJ, Zhang Y, Haselbach L. Improving flood inundation mapping accuracy using HEC-RAS modeling: a case study of the Neches River tidal floodplain in Texas. J Hydrol Eng 2024;29:5024011. https://doi.org/10.1061/JHYEFF.HEENG-6037.
[80] Zeiger SJ, Hubbart JA. Measuring and modeling event-based environmental flows: an assessment of HEC-RAS 2D rain-on-grid simulations. J Environ Manage 2021;285. https://doi.org/10.1016/j.jenvman.2021.112125.
[81] IPCC. Climate change 2023: synthesis report. In: Contribution of Working Groups I, II and III to the Sixth Assessment Report of the Intergovernmental Panel on Climate Change. Geneva, Switzerland; 2023. https://doi.org/10.59327/IPCC/AR6-9789291691647.
[82] Duperrin J, Godet M. Méthode de hiérarchisation des éléments d'un système: essai de prospective du système de l'énergie nucléaire dans son contexte sociétal. 1973.
[83] Isa M, Fauzi A, Susilowati I. Flood risk reduction in the northern coast of Central Java Province, Indonesia: an application of stakeholder's analysis. Jamba J Disaster Risk Stud 2019;11:1421–996. https://doi.org/10.4102/jamba.v11i1.660.
[84] Godet M. De la anticipación a la acción: manual de prospectiva y estrategia. Barcelona: Marcombo; 1993.
[85] Godet M, Durance P. Prospectiva Estratégica: problemas y métodos. Second. ed. Paris, France: Prospektiker; 2007.
[86] Peña LE, Zapata MA, Barrios M. Analytic hierarchy process approach for the selection of stream-gauging sites. Hydrol Sci J 2019;64:1783–92. https://doi.org/10.1080/02626667.2019.1672874.

[87] Van Dorp JR, Shittu E. The generalized two-sided beta distribution with applications in project risk analysis. J Stat Theory Pract 2023;17:1–27. https://doi.org/10.1007/s42519-023-00335-6.
[88] Uddin MN, Saiful Islam AKM, Bala SK, Islam GMT, Adhikary S, Saha D, et al. Mapping of climate vulnerability of the coastal region of {Bangladesh} using principal component analysis. Appl Geogr 2019;102:47–57. https://doi.org/10.1016/j.apgeog.2018.12.011.
[89] Márquez JD, Peña LE, Barrios M, Leal J. Detection of rainwater harvesting ponds by matching terrain attributes with hydrologic response. J Clean Prod 2021;296:126520. https://doi.org/10.1016/j.jclepro.2021.126520.
[90] Casacci S. Categorical principal component analysis. In: Maggino F, editor. Encyclopedia of quality of life and well-being research. Cham: Springer International Publishing; 2020. p. 1–2. https://doi.org/10.1007/978-3-319-69909-7_104643-1.
[91] Comoé H, Siegrist M. Relevant drivers of farmers' decision behavior regarding their adaptation to climate change: a case study of two regions in Côte D'ivoire. Mitig Adapt Strat Glob Chang 2015;20:179–99. https://doi.org/10.1007/s11027-013-9486-7.
[92] Sperman C. The proof and measurement of association between two things. Am J Psychol 1904;15:72–101. https://doi.org/10.2307/1412159.
[93] Caruso J, Clieff N. Empirical size, coverage, and power of confidence intervals for spearman's rho. Educ Psychol Meas 1997;57:637–54. https://doi.org/10.1177/0013164497057004009.
[94] Gaál L, Szolgay J, Kohnová S, Hlavcová K, Parajka J, Viglione A, et al. Dependence between flood peaks and volumes: a case study on climate and hydrological controls. Hydrol Sci J 2015;60:968–84. https://doi.org/10.1080/02626667.2014.951361.
[95] Blöschl G. Three hypotheses on changing river flood hazards. Hydrol Earth Syst Sci 2022;26:5015–33. https://doi.org/10.5194/hess-26-5015-2022.
[96] Marshall MR, Ballard CE, Frogbrook ZL, Solloway I, Mcintyre N, Reynolds B, et al. The impact of rural land management changes on soil hydraulic properties and runoff processes: results from experimental plots in upland UK. Hydrol Process 2014;28:2617–29. https://doi.org/10.1002/hyp.9826.
[97] Vargas LG. Reciprocal matrices with random coefficients. Math Model 1982;3:69–81. https://doi.org/10.1016/0270-0255(82)90013-6.
[98] Deschamps B, Boudreault M, Gachon P. Flooding: contributing factors to residential flood damage in Canada. Int J Disast Risk Reduct 2025;120:105348. https://doi.org/10.1016/j.ijdrr.2025.105348.
[99] Percival S, Teeuw R. A methodology for urban micro-scale coastal flood vulnerability and risk assessment and mapping. Nat Hazards 2019;97:355–77. https://doi.org/10.1007/s11069-019-03648-7.
[100] Gebremichael A, Gebremariam E, Desta H. GIS-based mapping of flood hazard areas and soil erosion using analytic hierarchy process (AHP) and the universal soil loss equation (USLE) in the Awash River Basin, Ethiopia. Geosci Lett 2025;12. https://doi.org/10.1186/s40562-025-00382-w.
[101] Xu Z, Yang W, Zhang X, Gu C, Shen L, Hu H. Satellite-based monitoring and hazard assessment of multiple flooding types in the Haihe River Basin induced by the July 2023 extreme rainstorm. J Hydrol 2025;663:134243. https://doi.org/10.1016/j.jhydrol.2025.134243.
[102] Fatemi MN, S.A., O, S.K., D, M., K, M., S, S., M. Physical vulnerability and local responses to flood damage in peri-urban areas of Dhaka, Bangladesh. Sustain 2020;12:1–23.
[103] Wetzel M, Schudel L, Almoradie A, Komi K, Adounkpè J, Walz Y, et al. Assessing flood risk dynamics in data-scarce environments—experiences from combining impact chains with Bayesian network analysis in the lower Mono River Basin, Benin. Front Water 2022;4:1–16. https://doi.org/10.3389/frwa.2022.837688.
[104] Bagheri-Gavkosh M, Panici D, Puttock A, Dauben T, Brazier RE. Hydrological analysis and impacts of natural flood management strategies: a systematic review. J Flood Risk Manag 2025;18:1–27. https://doi.org/10.1111/jfr3.70112.
[105] Shuka KAM, Wang K, Abubakar GA, Xu T. Impact of structural and non-structural measures on the risk of flash floods in arid and semi-arid regions: a case study of the Gash River, Kassala, eastern Sudan. Sustain 2024;16:1–23. https://doi.org/10.3390/su16051752.
[106] Xie Z, Shu B. Risk assessment and spatial zoning of rainstorm and flood hazards in mountainous cities using the random forest algorithm and the SCS model. 2025.
[107] Al-Hussein AAM, Hamed Y, Al-Timimy RS, Bouri S. Application of analytical hierarchy process and frequency ratio model for predictive flood susceptibility mapping using GIS for the Khazir River Basin, Northern Iraq. Iraqi Geol J 2023;56:118–38. https://doi.org/10.46717/igj.56.2E.9ms-2023-11-14.
[108] Erena SH, Worku H. Flood risk analysis : causes and landscape based mitigation strategies in Dire Dawa city. Ethiopia 2018;8.
[109] Dawson RJ, Ball T, Werritty J, Werritty A, Hall JW, Roche N. Assessing the effectiveness of non-structural flood management measures in the Thames estuary under conditions of socio-economic and environmental change. Glob Environ Chang 2011;21:628–46. https://doi.org/10.1016/j.gloenvcha.2011.01.013.
[110] López J, Francés F. Non-stationary flood frequency analysis in continental Spanish rivers, using climate and reservoir indices as external covariates. Hydrol Earth Syst Sci 2013;17:3189–203. https://doi.org/10.5194/hess-17-3189-2013.
[111] Visessri S, Ekkawatpanit C. Flood management in the context of climate and land-use changes and adaptation within the chao phraya river basin. J Disaster Res 2020;15:579–87. https://doi.org/10.20965/jdr.2020.p0579.
[112] Malgwi MB, Fuchs S, Keiler M. A generic physical vulnerability model for floods: review and concept for data-scarce regions. Nat Hazards Earth Syst Sci 2020;20:2067–90. https://doi.org/10.5194/nhess-20-2067-2020.